# The Anisotropic Nature of Singlet Fission in Single Crystalline Organic Semiconductors

Gang-Hua Deng<sup>1</sup>, Jesse B. Brown<sup>2</sup>, Haley Fisher<sup>2</sup>, Zhi-Chao Huang-Fu<sup>2</sup>, Yuqin Qian<sup>2</sup>, Tong Zhang<sup>2</sup>, Avetik Harutyunyan<sup>3</sup>, Hanning Chen<sup>4\*</sup>, Gugang Chen<sup>3\*</sup>, Yi Rao<sup>2\*</sup>

 <sup>1</sup>State Key Laboratory of Information Photonic and Optical Communications and School of Science, Beijing University of Posts and Telecommunications (BUPT), Beijing 100876, P. R. China
 <sup>2</sup> Department of Chemistry and Biochemistry, Utah State University, Logan, UT, 84322, United States
 <sup>3</sup>Honda Research Institute USA, Inc., San Jose, CA 95134, United States
 <sup>4</sup>Texas Advanced Computing Center, the University of Texas at Austin, Austin, TX 78758, United States

#### Abstract

The escalating global energy predicament implores for a revolutionary resolution—one that converts sunlight into electricity—holding the key to supreme conversion efficiency. This comprehensive review embarks on the exploration of the principle of generating multiple excitons per absorbed photon, a captivating concept that possesses the potential to redefine the fundamental confines of conversion efficiency, albeit its application remains limited in photovoltaic devices. At the nucleus of this phenomenon are two principal processes: multiple exciton generation (MEG) within quantum-confined environments, and singlet fission (SF) inside molecular crystals. The process of SF, characterized by the cleavage of a single photogenerated singlet exciton into two triplet excitons, holds promise to potentially amplify photonto-electron conversion efficiency twofold, thereby laying the groundwork to challenge the detailed balance limit of solar cell efficiency. Our discourse primarily dissects the complex nature of SF in crystalline organic semiconductors, laying special emphasis on the anisotropic behavior of SF and the diffusion of the subsequent triplet excitons in single-crystalline polyacene organic semiconductors. We initiate this journey of discovery by elucidating the principles of MEG and SF, tracing their historical genesis, and scrutinizing the anisotropy of SF and the impact of quantum decoherence within the purview of functional mode electron transfer theory. We present an overview of prominent techniques deployed in investigating anisotropic SF in organic semiconductors, including femtosecond transient absorption microscopy and imaging as well as stimulated Raman scattering microscopies, and highlight recent breakthroughs linked with the anisotropic dimensions of Davydov splitting, Herzberg-Teller effects, SF, and triplet transport operations in singlecrystalline polyacenes. Through this comprehensive analysis, our objective is to interweave the fundamental principles of anisotropic SF and triplet transport with the current frontiers of scientific discovery, providing inspiration and facilitating future ventures to harness the anisotropic attributes of organic semiconductor crystals in the design of pioneering photovoltaic and photonic devices.

**Key words**: Singlet fission, Multiexciton generation, Triplet transport, Single crystalline acenes, Vibronic coupling, Triplet Exciton Diffusion, Organic Semiconductors, Anisotropic Properties, Quantum Decoherence, Photon-to-Electron Conversion Efficiency, Herzberg-Teller Effects

Solar cells offer a promising, clean solution to the global energy crisis by converting incident solar radiation into electricity which can be stored and harnessed. Since their conception, their efficiency has been on an upward trajectory. The first generation of solar cells, typically polycrystalline or single-crystalline silicon, where a *pn*-junction is used to convert incident photons into electrical current. Due to their extended use and commercial optimization, first-generation photovoltaics are also some of the most efficient. However, they are still bulky, resource-demanding, and out dated. Second generation solar cells, thin film *pn*-junction systems, are made of amorphous silicon or other semiconductor thin films, constructed in multiple layers to maximize incident light utilization. Initially, second-genration cells possessed an economic advantage over their predecessors which compensated the slightly reduced conversion efficiency. However, this is not the case any more which has rendered most photovoltaics of this kind obsolete. The third genration of solar cells includes engineered materials such as those with multiple junctions, dye sensitization, quantum dots, perovskites, and organic semiconductors. These photovoltaics offer a wide range of applicability, efficiency, and affordability. One such branch of third-generation solar cells, organic semiconductors, may still yet achieve excellent conversion efficiency by overcoming the thermodynamic limit for single-junction solar cells of 30%. <sup>1</sup>

The third generation of solar cells is varied in the materials employed, from organic semiconductors to multijunction constructions and from dye molecules to quantum dots. Among the different means by which third generation solar cells can overcome this efficiency barrier is by generating more than one exciton, or electron-hole pair, per absorbed photon. The most general case of such a process is impact ionization (II), where an incident photon with excess energy generates a high-energy exciton, or hot carrier. This hot carrier can then collide with a nearby molecule and impart some of it excess energy to it, resulting in more than one generated exciton. Two more precise cases of greater-than-unity exciton conversion are known as multiple exciton generation (MEG) which occurs in quantum-confined inorganic systems, and singlet exciton fission (SF) wich occurs in some organic semiconductors such as acene crystals. Both MEG and SF have been applied to photovoltaic and photonic systems in recent years, and are sometimes even combined to further enhance overall device performance. For this reason, we believe that it is relevant to first give an outline of previous work covering MEG and SF as they apply to optoelectronic systems before comprehensively discussing the anisotropic nature of SF and related properties of acene single-crystals.

## 1. History of Singlet Fission in Organic Materials

Singlet fission (SF) emerges in molecular systems like chromophores. SF initiates when a high-energy photon creates a singlet state exciton, an exciton possessing energy approximately twice that of the triplet state. This singlet exciton then transitions into two triplet excitons, potentially enabling a photon-to-exciton conversion efficiency of 200%. Microscopically, this phenomenon proceeds from the formation of an electronically and spin correlated triplet biexciton,  $^{1}(TT)$ , followed by the dissociation into a spin-correlated but spatially separated triplet biexciton  $^{1}(T \cdots T)$ , namely quantum decoherence. Eventually, spin decoherence gives two spin-uncorrelated  $T_{1}$  excitons. The mechanism for SF is given by,  $^{2-8}$ 

$$k_{\rm F}$$
  $k_{\rm QD}$   $S_0 + S_1 \longrightarrow {}^1({\rm TT}) \stackrel{\leftarrow}{\hookrightarrow} {}^1({\rm T} \cdots {\rm T}) \longrightarrow {}^1{}_1 + {}^1{}_1$  (1)

where  $S_0$  represents a ground state,  $S_1$  is a singlet exciton,  $T_1$  is a triplet exciton,  $^1(TT)$  is the electronically and spin correlated triplet biexciton that has overall singlet spin, and  $^1(T\cdots T)$  is the spatially separated triplet biexciton with overall singlet spin. In the fission process, the  $S_1$  loses energy to an adjacent  $S_0$  such that both are converted to the triplet state at rate  $k_F$ , forming the correlated pair. With rate  $k_{QD}$ , the pair undergoes quantum decoherence (QD) to  $^1(T\cdots T)$  which can be further extracted as electrons for light-to-

energy conversion as . If  $S_1 > 2T_1$ , then the process is exothermic and favorable. If this is not the case, the SF process is endothermic and requires assistance in the form of additional energy or an intermediate state to be completed. The precise mechanisms for the formation of  $^1(TT)$  adn its dissociation into  $(T_1 + T_1)$  have been studied extensively depending on the material and are discussed in detail in the literature. Similar to MEG in inorganic semiconductors, SF is a potential way to increase photovoltaic efficiency.

The potential of SF to double photovoltaic output and overcome the thermodynamic limit of ~30% efficiency, <sup>12</sup> potentially boosting the photovoltaic power efficiency of a single junction solar cell to over 40%, makes it significant in the field. <sup>13, 14</sup> The origins of SF can be traced back to polyacene molecular crystals, initially employed to interpret exciton and fluorescence behaviors of anthracene under laser radiation, <sup>15</sup> and later confirmed through the explanation of nonradiative decay of crystalline tetracene. <sup>16</sup> While studies in the 1970s affirmed the presence of SF in tetracene <sup>17, 18</sup> and perylenes, <sup>19</sup> it was not until much later that value of SF in photovoltaics was recognized, triggering more research. <sup>20</sup> These benefits of SF include creating double the excitons compared to absorbed photons, spin-forbidden relaxation from the triplet state, and the triplet state's longer lifetime, providing an extended window for carrier separation. <sup>2</sup> A recent upsurge in SF research is evident, surpassing publications on MEG around 2015, as demonstrated in Figure 1. Over the past few years, many reviews have been published in the field of SF research. The first major review of the field was conducted by Smith and Michl in 2010, which provided a comprehensive overview of spin physics, chromophores, and spectroscopy in the field. <sup>2</sup> Since then, the field has made significant progress and expanded, resulting in the publication of numerous specialized reviews including several recent ones covering SF.<sup>21-23</sup>

The first application of SF in a potential photovoltaic device showcasing over 100% internal quantum efficiency (IQE) came to fruition in 2009,<sup>24</sup> with a multilayer organic semiconductor composed of pentacene and  $C_{60}$  components. Note that IQE pertains only to the conversion from one singlet to two triplets, excluding recombination post-SF.<sup>25</sup> In the case of pentacene, its exothermic SF process boosted the likelihood of increased QE. Thirty bilayers of pentacene and  $C_{60}$  comprised the absorptive material in this construct, and the compatible absorptions of these materials facilitated high absorption across almost the entire visible spectrum. This accomplishment motivated further SF research, aiming to incorporate such materials in next-gen solar cells. Following the influential review by Smith and Michl,<sup>2</sup> SF research gained substantial attention and progressed significantly. Another polyacene, tetracene, was later incorporated in an SF-based organic solar cell's design, paired with copper phthalocyanine and  $C_{60}$ . In this design, the phthalocyanine complex facilitated the transportation of generated triplet excitons from the tetracene layer to the  $C_{60}$  layer, broadening the absorption spectrum into the red wavelengths. This phthalocyanine addition also offset the voltage potential reduction by SF. This breakthrough introduced another compatible layer to the polyacene/bucky ball system for enhanced solar conversion efficiency. It also showed that a "blended" tetracene/ $C_{60}$  layer retained efficient SF activity while simplifying fabrication.

In terms of SF materials, tetracene has a very useful triplet excitation energy of 1.2 eV.<sup>2</sup> The first steadfast use of tetracene for SF in photovoltaics was in 2014, where it obtained an IQE of nearly 130%.<sup>27</sup> This report also demonstrated that thicker layers of tetracene must be used than could be with pentacene as the SF process is considerably slower. On the other hand, it was later observed that a tetracene polymer exhibited much faster SF than the monomer thin film while retaining high triplet excitation energy.<sup>28</sup> Tetracene has also been introduced into a layered device with silicon, however it did not provide any notable improvement to the system.<sup>29</sup> Luckily, there was a breakthrough in SF devices in 2019 which used subnanometer hafnium oxynitride between the tetracene and silicon layers and boasted an impressive 5.1% power efficiency and 13.3% EQE, reinstating tetracene as a viable SF material in solar cell devices. Rubrene, a polycyclic aromatic hydrocarbon, has also been used in SF devices with some potential. Using a different organic layer to generate a singlet which would then generate two triplets in the rubrene layer, it was shown that the addition of rubrene more than doubled the EQE, reaching 27.6%.<sup>30</sup> This efficiency was optimized even further by combining rubrene with C<sub>60</sub> to 30% EQE.<sup>31</sup> Interestingly, while triplet-triplet annihilation

(TTA) was found to be significant cause for decreased efficiency in rubrene, the effect actually promoted charge separation in amorphous rubrene, improving its EQE over crystalline rubrene where SF was low.<sup>32</sup> Returning the focus to pentacene, the first demonstration of EQE >100% was in 2013.<sup>33</sup> This device used a pentacene thin film for SF, a poly(3-hexylthiophene) (P3HT) layer for exciton confinement, and a fullerene acceptor layer, 109% EQE was achieved after obtaining a 160% IQE from nearly 200% triplet yield. Another source of loss in efficiency for photovoltaics, with or without SF, is simply through the reflection of incident light by the device surface.

SF also offers avenues for enhancing photonic devices.<sup>34-39</sup> To boost SF performance in pentacene, PbS and PbSe nanocrystals have been successfully integrated into layered devices by capturing triplet electrons through visible light and IR absorption.<sup>34</sup> The system's efficiency was further improved by adjusting the nanocrystals' size to align their energy gap closely with the triplet state.<sup>36, 37</sup> This configuration, using a pentacene derivative, set a new record with 4.8% power efficiency. In an innovative approach, an organic (pentacene) and inorganic (silicon) photovoltaic cell were combined to achieve a maximum power efficiency of 5.1%, with the cells connected electrically in parallel but optically in series, so the light passed first through the organic layer.<sup>40</sup> In a later instance, rubrene was used to generate triplet excitons which were then transferred to a receptor that provided radiative recombination, producing photons in the near-IR at over 100% efficiency.<sup>41</sup> With applications of SF devices branching far and wide into photovoltaics and photonics, this process must be robustly understood for as many materials as possible to continue to push forward in applications frontiers.

Most of the studies of SF focus on polycrystalline thin films of organic semiconductors. The photophysics observed in polycrystalline samples may differ from those in single crystals due to various factors, such as the presence of defect sites and interfaces that could accelerate SF. Single crystals, conversely, provide certain advantages. These include minimal defects, which promote more accurate and reliable experimental results, and greater comparability with theoretical models, allowing for deeper insights into the photophysics of SF. Furthermore, due to the continuous crystal axes, single crystals facilitate the observation of anisotropy more readily. This could result in a greater dependence of the excited state transition dipole orientation on the crystal orientation, offering a new dimension of investigation.

This review will focus on these anisotropic characteristics in polyacene single crystals. Specific topics of focus will include Davydov splitting, anisotropic SF, and anisotropic exciton diffusion, which provide a fresh perspective on the mechanisms of SF and potential paths for optimization in photovoltaic applications. We will start with a thorough theoretical analysis of SF. Then, the anisotropic effects in single crystalline organics will be discussed as they pertain to Davydov splitting, Herzberg-Teller effects, SF, and triplet diffusion. Lastly, we will provide our perspective on current unanswered questions facing SF research.

# 2. Theory of Singlet Fission

## 2.1 Functional Mode Singlet Fission Theory

Based on functional mode analysis, <sup>42</sup> a theory has been developed to better understand the process of electron transport in semiconductor systems as well as the involvement of vibronic coupling strengths therein, which is referred to as functional mode electron transfer theory (FEMET). <sup>43</sup> FEMET has been successfully extended to apply to hot electron transfer under nonthermalized conditions. <sup>44</sup> More precisely, the electron injection rate from a photoexcited dye molecule into anatase TiO<sub>2</sub> was found to depend on incident photon energy. Here we extend this theory to model SF processes, including multiple spin configurations which participate in the generation of multiple excitons.

The reaction coordinate,  $\vec{V}$ , of an electron transfer or spin transition process between donor,  $\Psi_D$ , and acceptor,  $\Psi_A$ ,, diabatic states can be formulated as a linear combination of all vibrational normal modes:<sup>43</sup>

$$\vec{V} = \sum_{i=1}^{N_{vib}} c_i \, \vec{V}_i \,, \tag{2}$$

where the expansion coefficient,  $c_i$ , indicates the relative contribution of the  $i^{th}$  vibrational mode,  $\vec{V}_i$ , to the degeneracy of vibronic energy that is required for a non-radiative transition. Here, the vibrational modes were determined by diagonalizing the mass-weighted cross-correlation matrix of atomic displacements in a molecular dynamics trajectory. By following the functional mode analysis method,  $^{42}\vec{V}$  is ascertained through maximization of the Pearson's correlation coefficient, R, which is defined as

$$R = \frac{\operatorname{cov}(p_{\overline{V}}(t), \Delta E_{DA}(t))}{\sigma_{\overline{V}} \sigma_{\Delta E_{DA}}},$$
(3)

where  $p_{\vec{V}}(t) = (\vec{r}(t) - \langle \vec{r} \rangle) \cdot \vec{V}$  is the projection of instantaneous nuclear configuration  $\vec{r}(t)$  on  $\vec{V}$ ,  $\Delta E_{DA}(t) = E_D(t) - E_A(t)$  is the instantaneous diabatic energy gap,  $\operatorname{cov}\left(p_{\vec{V}}(t), \Delta E_{DA}(t)\right)$  is the covariance function between  $p_{\vec{V}}$  and  $\Delta E_{DA}$ , with their standard deviations denoted as  $\sigma_{\vec{V}}$  and  $\sigma_{\Delta E_{DA}}$ , respectively. The search for the maximum value of R reduces to solving a set of linearly coupled equations:

$$\sum_{i=1}^{N_{vib}} c_i \text{cov}\left(p_{\vec{V}_i}(t), p_{\vec{V}_j}(t)\right) = \text{cov}\left(\Delta E_{DA}(t), p_{\vec{V}_j}(t)\right) \qquad j = 1, ..., N_{vib}.$$
(4)

Due to the multiexciton character of the acceptor,  $^1(T_1T_1)$  is constructed through a multiconfigurational constrained density functional theory-based approach.  $^{45, 46}$  To be specific, a spin-polarized Hartree potential was applied to a pair of adjacent chromophore molecules to achieve a net spin difference of  $^{+4}$  (or  $^{-4}$ ) between them as quantified by Becke population analysis.  $^{47}$  The resulting molecular orbitals were then adopted as building blocks to construct the six constituent spin configurations of the  $^{1}(T_1T_1)$  state through spin flips. Construction of the donor  $S_0S_1$  state was accomplished by using linear-response time-dependent density functional theory (LR-TDDFT) to determine its molecular orbitals via excitation of multiple Kohn-Sham electron-hole pairs.

Because of thermodynamic reversibility, the free energy gap between the  $S_0S_1$  and  $^1(T_1T_1)$  states,  $\Delta G_{S_0S_1\to^1(T_1T_1)}$  is given by

$$\Delta G_{S_0 S_1 \to {}^{1}(T_1 T_1)} = \Delta G_{S_0 S_0 \to {}^{1}(T_1 T_1)} - \left( \Delta E_{S_0 S_0 \to S_0 S_1} - \Delta E_{TR} \right), \tag{5}$$

where  $\Delta G_{S_0S_0 \to ^1(T_1T_1)}$  is the gap between  $S_0S_0$  and  $^1(T_1T_1)$ ,  $\Delta E_{S_0S_0 \to S_0S_1}$  is the vertical excitation energy, and  $\Delta E_{TR}$  is the thermal relaxation energy at  $S_0S_1$ . Although it is trivial to calculate both  $\Delta E_{S_0S_0 \to S_0S_1}$  and  $\Delta E_{TR}$  using LR-TDDFT,<sup>48</sup> the thermodynamic integration method<sup>49</sup> must be utilized to compute  $\Delta G_{S_0S_0 \to ^1(T_1T_1)}$  through a linearly mixed Hamiltonian,  $H_{mix}(\eta)$ , that spans over eleven sampling windows of 10-ps each with evenly spaced values of  $\eta$ :

$$H_{mix}(\eta) = (1 - \eta)\hat{H}_{S_0S_0} + \eta \hat{H}_{T_1T_1}. \tag{6}$$

After sampling the gradient of  $H_{mix}(\eta)$  along  $H_{mix}(\eta)$ ,  $\Delta G_{S_0S_0 \to {}^1(T_1T_1)}$  is obtained by discrete summation:

$$\Delta G_{S_0 S_0 \to 1(T_1 T_1)} = \sum_{i=1}^{N_{\eta}} \left( \frac{\partial H_{mix}(\eta)}{\partial \eta} \right)_{\eta_i} \Delta \eta_i . \tag{7}$$

Without any additional simulation, the reorganization energy,  $\lambda$ , can be also deduced:

$$\lambda = \langle H_{mix}(\eta = 1) - H_{mix}(\eta = 1) \rangle_{\eta = 0} + \Delta G_{S_0 S_0 \to {}^1(T_1 T_1)}. \tag{8}$$

Moreover, using the extended Slater-Condon rule<sup>50</sup> for non-orthonormal molecular orbitals (see Supporting Information),  $\langle {}^{1}(T_{1}T_{1})|\hat{H}_{0}|S_{0}S_{1}\rangle$  is simplified to the sum of couplings between selected spin configurations:

$$\langle {}^{1}(T_{1}T_{1})|\widehat{H}_{0}|S_{0}S_{1}\rangle = \sqrt{\frac{3}{2}} \left( \left( \begin{matrix} + & \uparrow & |\widehat{H}_{0}| & \uparrow \\ + & \uparrow & |\widehat{H}_{0}| & \uparrow \\ + & + & \downarrow \end{matrix} \right) + \left( \begin{matrix} \uparrow & + & |\widehat{H}_{0}| & \uparrow \\ \uparrow & + & |\widehat{H}_{0}| & \uparrow \\ \uparrow & + & \downarrow \end{matrix} \right). \tag{9}$$

In order to ensure rigorous orthogonality between  ${}^{1}(T_{1}T_{1})$  and  $S_{0}S_{1}$ , a revised expression<sup>51</sup> that affords orbital renormalization is adopted:

$$\langle {}^{1}(T_{1}T_{1})|\widehat{H}_{0}|S_{0}S_{1}\rangle = \sqrt{\frac{3}{2}} \left(\frac{2E_{TS} - S_{TS}(E_{T} + E_{S})}{2(1 - S_{TS}^{2})}\right),\tag{10}$$

where

$$E_{TS} = \begin{pmatrix} + & \uparrow & |\widehat{H}_{0}| & \uparrow \\ + & \downarrow & |\widehat{H}_{0}| & \downarrow \\ + & \downarrow &$$

Once the free energy gap,  $\Delta G_0$ , reorganization energy,  $\lambda$ , and electronic coupling strength, J, associated with the  $S_0S_1 \to {}^1(T_1T_1)$  transition are all determined, we are ready to evaluate the overall SF rate,  $k_{SF}$ , using either the Jortner formula for strong vibronic coupling ( $\lambda \gg \hbar \omega$ ) or the energy-gap law for weak vibronic coupling ( $(\lambda \ll \hbar \omega)$ ).<sup>43</sup>

# 2.2 Perturbation Theory for Mediated Coherent Vibronic Transition

According to Fermi's golden rule, the direct transition rate,  $k_{i\rightarrow f}$ , between initial and final vibronic states is given by the first-order perturbation theory:

$$k_{i \to f} = \frac{2\pi}{\hbar} \langle \varphi_e^i | \widehat{H} | \varphi_e^f \rangle^2 \langle \varphi_v^i | \varphi_v^f \rangle^2 \rho_f, \tag{12}$$

where  $\varphi_e$  and  $\varphi_v$  denote the electronic and vibrational wavefunctions, respectively, and  $\rho_f$  is the density of states. Specifically, the electronic coupling strength can be quantified as  $J = \langle \varphi_e^i | \widehat{H} | \varphi_e^f \rangle$ , whereas the vibrational wavepacket overlap, or the so-called Franck-Condon factor, can be expressed as  $FC = \langle \varphi_v^i | \varphi_v^f \rangle^2$ . If the same orthogonal basis vectors,  $\{v_i\}$ , are adopted for both  $\varphi_v^i$  and  $\varphi_v^f$ ,

$$FC = \sum_{j} \sum_{j} \langle v_j^i | v_{j}^f \rangle^2 = \sum_{j} \langle v_j^i | v_j^f \rangle^2, \tag{13}$$

enabling the decomposition of FC onto individual vibrational modes. Interestingly, if a particular vibrational mode,  $v_j$ , is orthogonal to the designated reaction coordinate,  $\vec{R}_{if}$ , associated with the nonadiabatic  $i \to f$  transition, the corresponding mode-resolved  $FC_{ij} = \langle v_j^i | v_j^f \rangle$  vanishes due to the complete directional misalignment between the initial and final vibrational wavepackets. By contrast,  $FC_{ij}$  is maximized when  $v_j$  coincides with  $\vec{R}_{if}$ . Therefore, any deviation of  $v_j$  with respect to  $\vec{R}_{if}$  can be treated as an out-of-plane rotation of the vibrational wavepackets that results in their diminished overlap and thus a reduced  $FC_i$ . If  $\vec{R}_{if}$  itself is expressed as a linear combination of  $\{v_i\}$ :

$$\vec{R}_{if} = \sum_{i} c_i \vec{v}_i \,, \tag{14}$$

the rotation angle,  $\theta_k^{rot} = c_k$ , due to the unavailability of a single vibrational mode,  $v_k$ , is given by  $\theta_k^{rot} = \sin^{-1} c_k^2$  where  $c_k$  reflects the mode's relative vibronic coupling strength. In a similar fashion, if the  $i \to f$  transition is coherently mediated by a non-degenerate intermediate vibronic state, m, the second-order perturbation form of the Fermi's golden rule reads:

$$k_{i\to f}^{m} = \frac{2\pi J_{im}^{2} J_{mf}^{2} F C_{im} F C_{mf}}{\hbar \Delta E_{mi}^{2}} \rho_{f} , \qquad (15)$$

where  $\Delta E_{mi} = E_m - E_i$  is the energy gap that governs the strength of vibronic mixing between the initial and final states facilitated by the intermediate. Interestingly, since

$$FC_{im}FC_{mf} = \sum_{j} \langle v_j^i | v_j^m \rangle^2 \langle v_j^m | v_j^f \rangle^2 , \qquad (16)$$

only the vibrational modes that align well with both  $\vec{R}_{im}$  and  $\vec{R}_{mf}$  can leave appreciable footprints during this two-step coherent process. From a practical standpoint, the intermediate state, m, serves as a "coherence filter" that blocks the transfer of coherence for all vibrational modes that are uncritical to the mediated  $i \rightarrow f$  transition. Experimentally, the "coherence filter" could be implemented by selectively polarized photoexitation in anisotropic single crystals.

# 3. Experimental Methods for Singlet Fission

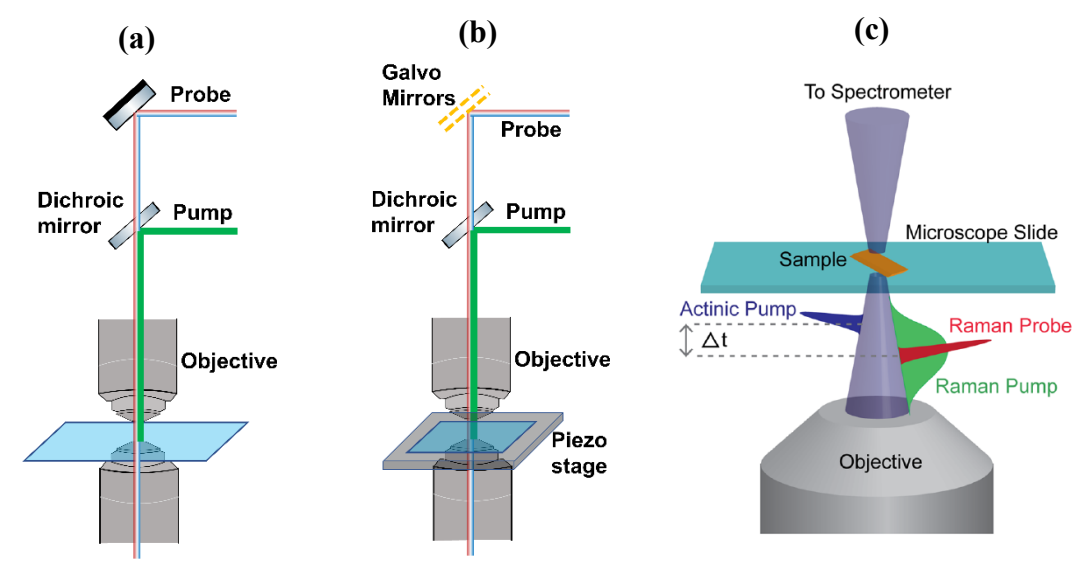


**Figure 1.** Schematic diagrams of (a) transient absorption microscope, (b) transient absorption imaging, and (c) femtosecond stimulated Raman scattering microscope setups.

Reproduced from [A. A. Cassabaum, K. Bera, C. C. Rich, B. R. Nebgen, S. Y. Kwang, M. L. Clapham, and R. R. Frontiera, "Femtosecond stimulated Raman spectro-microscopy for probing chemical reaction dynamics in solid-state materials," J. Chem. Phys. **153** (2020) 030901.] with the permission of AIP Publishing.

With the main concern of this article being the anisotropic nature of organic semiconductor materials, methods for investigation must be able to accurately define crystal axes. In acene single crystals, individual crystalline domains suitable for transmission spectroscopy measurements have sizes on the order of tens of microns. <sup>52-54</sup> However typical optical spectroscopy setups employ spot sizes greater than 100 µm, which would result in signal mixing among multiple crystal domains and not obtain the spatial resolution required to observe anisotropic behaviors. For these reasons, common methods for polarization angle-resolved spectroscopy of crystalline acenes often employ microscope objectives to achieve micron-scale spatial resolution. Here we will briefly describe the principles of transient absorption and femtosecond stimulated Raman microscopy methods. <sup>52-57</sup>

# 3.1 Transient Absorption Microscopy and Imaging

TA microscopy setups are similar, with additional measures to control the time at which the pump and probe lights are incident on the sample. 53,54 With TA being a method for observing electronic properties of excited states, it is useful to have a reference of the absorption or transmission spectra of the material in the UV-vis range. A schematic of a general TA microscope is shown in Figure 1(a). First, a seed femtosecond laser is divided to generate the pump and probe pulses. Different methods are used to obtain the desired wavelength of the pump pulse, such as an optical parametric amplifier (OPA). The pump pulse is also directed through a motorized translation stage which provides precise adjustment of the optical path length, thereby controlling pump-probe temporal delay. It is often desirable to have a broadband probe pulse, so measures are taken to generate a white light continuum from the original seed laser. The pump and probe pulses with controlled polarizations are then directed collinearly through the microscope objective to the sample. Another microscope objective is used to collect the transmitted probe light which is then directed to the detector. Precise synchronization of the laser, an optical chopper, and the detector allow the collection of absorption (or transmission) spectra with and without pumping the sample, which allows the user to then calculate the change in absorption (or transmission) of the sample with respect to the pump pulse. An

additional reference is sometimes used in TA experiments which redirects a weak portion of the probe light around the sample and to the detector to provide a reference of the incident spectrum for every collected sample spectrum. To achieve sample imaging in the same TA microscopy setup, beam splitters are inserted into the collinear light path before the sample to introduce an illumination source which is directed to its own separate camera for optical image collection.<sup>53, 54</sup> To collect UV-Visible spectra for single crystals, a lamp and/or LED light with tunable intensities are usually aligned into the microscopy setup, and measurements can be taken before the sample to obtain the desired polarization of the incident light.<sup>52</sup> The illumination is then focused through a microscope objective to a spot with a diameter of tens of µm, striking the sample normal to the surface. A collection objective is then used to gather the transmitted light before it is directed to a detector such as a spectrometer fitted with a charge-coupled device (CCD).

TA imaging is usually used to study exciton diffusion and transport, and spatial heterogeneity with microscopic resolution in a sample.<sup>58, 59</sup> A schematic of a general TA imaging microscope is shown in Figure 1(b). Instead of employing a broadband probe, a narrowband pulse is used to study specific regions of the TA spectrum. To study exciton diffusion and transport, the probe pulse is directed through a pair of galvanometer mirrors as shown in Figure 1(b), which provides minute changes in the angle of the incident light. Such small changes are made to systematically illuminate different parts of the sample. The subsequent TA signal is then detected by a photodiode and its responses are correlated with the galvanometer position to compile a TA image map. To study structural heterogeneity in a sample, the pump and probe pulses are kept stationary, and the sample is moved using a piezoelectric translation stage. This allows different regions of the sample to be investigated by the TA microscope and an image is compiled to map out is characteristics. Instruments for exciton diffusion studies have a higher spatial resolution by design while those studying heterogeneity cover more area to investigate the sample on a slightly larger microscopic scale.<sup>58-62</sup>

# 3.2 Femtosecond Stimulated Raman Microscopy

Femtosecond stimulated Raman spectroscopy (FSRS) uses ultrafast laser pulses to study the excited states of a material by observing changes in vibrational modes of an excited material.<sup>63, 64</sup> Opposed to TA and other electronic techniques, FSRS can be used to investigate vibrational dynamics in SF systems.<sup>65</sup> A schematic of an FSRS microscope is shown in Figure 1(c). FSRS employs three incident laser pulses: an actinic pump which excites an electronic mode of the sample as the TA pump does, a Raman pump, and a Raman probe. In this case, the difference in frequency between the Raman pump and probe pulses is near a resonant frequency of structural modes in the sample. Both Raman and actinic pump pulses pass through individual translation stages to control their temporal delay with respect to the white light Raman probe. The three polarization-controlled pulses are collinearly incident on the sample through a microscope objective. The FSRS signal and probe are then collected and directed to a spectrometer and CCD for spectral detection. The advantage of microscopic FSRS is that it affords the ability to visualize structural differences and surface defects while precisely orienting the sample's crystal axis.

## 4. Singlet Davydov Splitting in Tetracene, Pentacene and Hexacene

# 4.1 Structural Properties of Tetracene, Pentacene, and Hexacene

 to hexacene. For tetracene, the singlet state lies at approximately 2.32 eV, while its triplet state is at about 1.25 eV. Pentacene has a singlet state energy of around 1.86 eV and a triplet state energy of roughly 0.86 eV. Hexacene, the larger acene among the three, has a singlet state energy of about 1.46 eV and a triplet state energy level close to 0.5 eV. Their chemical stability decreases with an increasing number of benzene rings, making pentacene and hexacene more susceptible to oxidation and degradation in ambient conditions than tetracene. Their extended pi-conjugation allows for strong electronic interactions between the molecules and facilitates efficient SF. Efficient SF is also facilitated by their relatively low-lying triplet state energy. Additionally, these materials are absorptive in the visible region, making them attractive for use in solar energy conversion devices. Additionally these shared properties, there are also differences in the SF behavior of tetracene, pentacene, and hexacene, which depend on factors such as crystal packing and molecular morphology. Understanding and optimizing these differences can lead to improved SF performance and the development of more efficient and scalable solar energy conversion technologies.

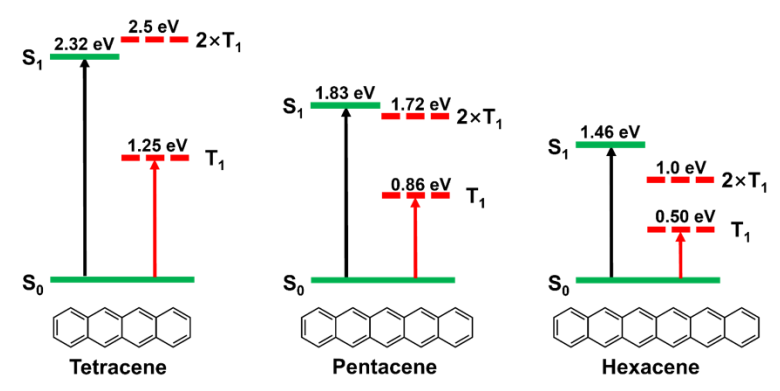


**Figure 2.** Energy level diagrams depicting the singlet and triplet energies of tetracene, pentacene, and hexacene.

## 5.2 Basic Concept of Singlet Davydov Splitting

Davydov splitting (DS) was defined as "the splitting of bands in the electronic or vibrational spectra of crystals due to the presence of more than one (interacting) equivalent molecular entity in the unit cell" by IUPAC. 76, 77 This coupling leads to a splitting of the energy levels of the excitations, which can have important implications for the optical and electronic properties of the crystal. The splitting is determined by different spatial orientations of anisotropic molecules in the crystal. 78 The magnitude of this splitting depends on several factors including temperature and pressure. At low temperatures and high pressures, for example, the splitting can be significantly larger than at standard temperature and pressure. In molecular crystals with more than one molecule per unit cell basis, the interaction of translationally inequivalent molecules leads to DS in the excitonic states. This splitting results in not only distinct energy levels but also different polarizations, which are the manifestation of the crystal's symmetry or the structural anisotropy of the crystal. For acenes, the existence of two non-equivalent molecules per unit cell in these crystals leads to two optical transitions primarily polarized along the two directions of the herringbone *ab*-plane as shown in Figure 3(a).

DS with excitation normal to the *ab*-plane ranges approximately 630 cm<sup>-1</sup> (0.078 eV) in tetracene,<sup>69, 81, 82</sup> roughly 1100 cm<sup>-1</sup> (0.136 eV) in pentacene<sup>52, 83</sup> and 1160 cm<sup>-1</sup> (0.144 eV) in hexacene<sup>53, 84</sup> for the lowest vibronic (0–0) transition. An extensive analysis of the DS in oligoacenes was previously conducted by Schlosser and Philpott,<sup>85</sup> who concluded that a reasonably good agreement with experiment could only be

achieved by including higher-lying Frenkel (i.e., molecular) excitations for tetracene and pentacene. However, Schuster et al. <sup>86</sup>, employing inelastic electron scattering on pentacene crystals, revealed the limitations of a purely Frenkel exciton model in accounting for the exciton dispersion, suggesting the need to incorporate coupling to intermolecular charge-transfer (CT) excitons. In crystalline oligoacenes, the presence of CT excited states was initially demonstrated by Sebastian et al. <sup>87,88</sup> through electro-absorption experiments, and more recently, by Zhu and colleagues using time- and angle-resolved two-photon photoemission spectroscopy. <sup>89,90</sup> In fact, a strong CT contribution to the DS of tetracene was suggested by the theoretical work of Petelenz et al. <sup>91</sup> in the late 1980s. A more recent theoretical analysis for pentacene by Tiago et al. <sup>92</sup> also highlighted the significance of CT to DS. However, vibronic coupling, which greatly influences DS, was not included in these two studies. More recently, more quantitative studies by Spano and co-workers were able to reproduce both 0-0 DS as well as 0-*n* vibronic intensities for oligoacenes by considering particle states, Frenkel bands, and vibronic CT states. <sup>52,93</sup> In the following section, the details of the singlet Davydov splitting in tetracene, pentacene and hexacene are reviewed.

# 5.3 Singlet Davydov Splitting in Tetracene Single Crystals

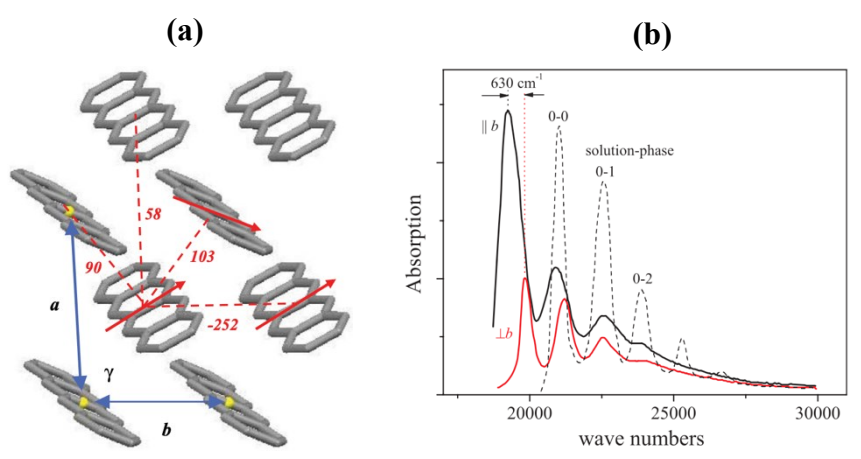


**Figure 3.** (a) Diagram of the crystal structure of crystalline tetracene with the a and b axes are slightly obtuse at  $\gamma = 94^{\circ}$ , (b) comparison of solution-phase (dashed) and crystalline absorption spectra along (solid black) and perpendicular to (solid red) the b-axis showing Davydov splitting of 630 cm<sup>-1</sup>.

Reproduced from [H. Yamagata, J. Norton, E. Hontz, Y. Olivier, D. Beljonne, J. L. Brédas, R. J. Silbey, and F. C. Spano, "The nature of singlet excitons in oligoacene molecular crystals," J. Chem. Phys. **134** (2011) 204703.] with the permission of AIP Publishing.

In solution, the absorption spectrum of tetracene shows a single peak at around 435 nm, <sup>81</sup> corresponding to the lowest energy singlet excited state. However, in crystalline form, this transition is represented by two distinct peaks at around 435 nm and 455 nm, <sup>81, 93</sup> as shown in Figure 3(b). This splitting is known as Davydov splitting (DS) and it arises from the coupling between electronic excitations and lattice vibrations. The nature of this coupling depends on several factors, including the crystal structure and orientation, as well as the nature of the electronic excitations themselves. The absorption spectra of tetracene single crystal was first reported in the 1950's <sup>77</sup> and the DS of its 0-0 band was found to be 575 cm<sup>-1</sup> (0.071 eV). In 1965, Ohigashi *et al.* studied the effect of pressure on DS in tetracene single crystals. <sup>79</sup> They found an increase in DS with increasing pressure, where the observed value was 200 cm<sup>-1</sup> (0.025 eV) under the pressure of 5.2 kbar. In 1969, Philpott investigated the contribution of dipole-dipole interactions to the DS of various molecules including tetracene. <sup>94</sup> Using the classical theory of exciton states, the Bose character of molecular excitons was assessed and the calculated DS values aligned well with experiments for anthracene and

tetracene and suggesting the importance of dipole-dipole interactions in DS. Schlosser and Philpott <sup>85</sup> conducted a more comprehensive analysis of the DS in oligoacenes and found that, for tetracene, the DS is mainly influenced by crystal-induced mixing with higher-lying Frenkel excitations. It was found that splitting is dependent on both dipole-dipole and nonpolar interactions.

In tetracene crystals, it has been shown that there is a significant charge transfer (CT) character to the lowest energy exciton. <sup>89, 90</sup> This indicates a transfer of electron density from one part of the molecule to another upon excitation. This CT character leads to an increased sensitivity to lattice vibrations, which in turn leads to larger DS. Recently, DS in tetracene crystals was re-examined by Yamagata *et al.* <sup>93</sup> Using all Frenkel couplings, calculated spectra revealed a -32 cm<sup>-1</sup> vibronic band for the lowest energy transition DS in tetracene, much lower than previous measurements. Additionally, the predicted spectrum had the incorrect sign. However, when Frenkel-CT coupling is considered, the agreement with the experimental results is greatly improved, giving a value of 601 cm<sup>-1</sup> (0.075 eV) compared to the experimental value of 631 cm<sup>-1</sup> (0.078 eV). Such inclusion also resulted in the relative spectral intensities of the 0-*n* vibronic components being nearly reproduced. The theoretical study shed new light on DS by providing detailed calculations of the exciton properties in tetracene crystals.

# 5.4 Singlet Davydov Splitting in Pentacene Single Crystals

Although the optoelectronic properties of pentacene have received much attention, few reports of its polarized absorption spectra have been made. <sup>83, 95, 96</sup> Such published spectra are challenging to analyze beyond the 0-0 DS, which is reportedly 1000-1100 cm<sup>-1</sup> (0.124-0.136 eV). In a recent study, the polarization dependence of the absorption spectrum in crystalline pentacene was examined by Hestand et al.<sup>52</sup> Figure

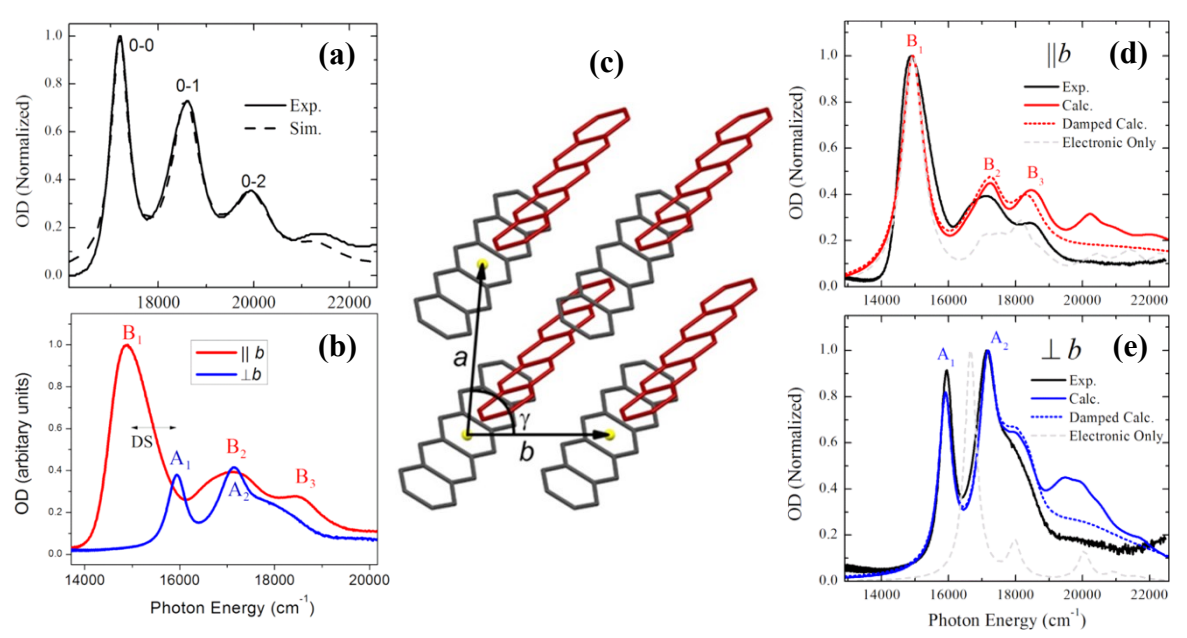


**Figure 4.** (a) Experimental and calculated absorption spectra of solution phase pentacene, (b) polarized absorption spectra of crystalline pentacene along the *a* and *b* crystal axes exhibiting Davydov splitting (DS), (c) crystalline structure of pentacene viewed along its *c*-axis, comparison of experimental and simulated polarized absorption spectra of pentacene single crystals along (d) and perpendicular to (e) the *b*-axis.

Reproduced with permission from J. Phys. Chem. C. **119** (2015) 22137. Copyright 2015 American Chemical Society.

4(a) displays the absorption spectra of pentacene in the solution phase and compares experimental and simulated results. A vibrational progression around 17,000 cm<sup>-1</sup> (2.11 eV) can be observed which is

associated with a vibrational energy of  $1380 \text{ cm}^{-1}(0.171 \text{ eV})$ , the symmetric ring stretching mode. Figure 4(b) compares the experimental absorption spectra for crystalline pentacene samples along and normal to the *b*-axis. The crystal structure of pentacene is shown in Figure 4(c) for clarity.

Using a Frenkel/CT Holstein-style Hamiltonian, the polarized absorption spectra of crystalline pentacene were calculated along and normal to the b-axis. The simulated and experimental spectra are compared in Figures 4(d) and (e). The calculated spectra qualitatively align with the experimental data for both polarizations and capture both DS and shape properties including peak positions and intensity ratios. From these observations, it was determined that in oligoacenes, generally, upper and lower Davydov component polarizations depend on the relative signs of the electron and hole integrals which connect molecules in sublattices. It was also shown that elevated CT content in  $S_1$  was responsible for DS along the b-axis which agrees with unpolarized absorption spectra.

# 5.5 Singlet Davydov Splitting in Hexacene Single Crystals

Polarized reflection experiments were conducted on hexacene single crystals in 2014 by Busby et al. to investigate its DS character. He was found that the intensities of the peaks at 1.44 and 1.60 eV are dependent on polarization, asserting the presence of a Davydov doublet of 160 meV DS energy. Possibly indicating a high degree of CT in hexacene. The DS value of hexacene is greater than those of tetracene and pentacene which are about 80 and 130 meV, respectively. Polarization-dependent reflection spectroscopy has also been conducted on single crystalline hexacene at cryogenic temperatures by Chernikov et al., resulting in even higher DS energy. After using a multi-Lorentzian model to quantitatively analyze the anisotropic transitions, it was suggested that the response indicates a significant dispersion in the electronic band structure that increases intermolecular interactions. The DS of 180 meV of hexacene single crystals at low temperatures furthers the strong CT character of the low-lying excitations.

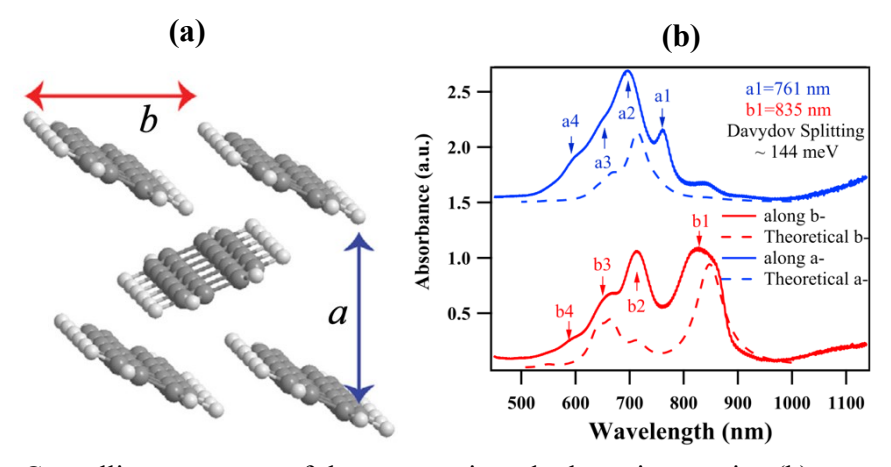


**Figure 5.** (a) Crystalline structure of hexacene viewed along its c-axis, (b) comparison of experimental (solid) and simulated (dashed) absorption spectra of single-crystalline hexacene along the a (blue) and b (red) axes.

Reproduced with permission from iScience 19 (2019) 1079. Copyright 2019 Elsevier.

Single-crystalline hexacene was also recently investigated using polarization-resolved transmission spectra. The crystalline hexacene triclinic unit cell is shown in Figure (a). Using a transient absorption microscope, the absorption spectra shown in Figure 5(b) were collected along the *a*- and *b*- axes which are displayed along with their theoretical counterparts. It should be noted that the *a*- and *b*-axes are reversed compared to the previously shown pentacene structure. A clear anisotropy is observed between the perpendicularly collected spectra shown in Figure 5(b). Comparing the al and bl peaks at 761 and 835 nm,

respectively, reveals a DS shift of 144 meV which is interestingly lower than that observed in the reflection experiments.

# 5.6 Herzberg-Teller Effects in Tetracene, Pentacene, and Hexacene

Vibronic coupling has a major impact on the process of SF in crystalline acenes and is manifested through the Herzberg-Teller (HT) effect. <sup>56, 57, 97-100</sup> The selection rules of vibrationally resolved electronic transitions depend heavily on molecular symmetry, especially when the molecular dependence of the electronic wavefunction is treated with Franck-Condon (FC) factors, FC/HT interference, and HT coupling. Accordingly, calculations have shown that HT considerations can greatly impact the photophysical description of polyacenes, where first- and second-order photoluminescence quantum yield calculations were contradictory to each other for naphthalene, anthracene, and tetracene. <sup>101</sup> It was shown that although all three acenes exhibited a quantum yield near 100% at the FC point, the inclusion of HT effects resulted in values near 10% for anthracene and tetracene, but that for naphthalene was around 90%. Further investigation showed that the lack of consideration of HT effects resulted in the overestimation of efficiency due to inadequate accounting for strong second-order contributions. Such a strong impact on the photophysical description of acenes indicates that HT effects should also be considered in SF scenarios for polyacenes.

Considerations have also been made to investigate the HT-effect on the vibrationally-resolved absorption of pentacene single-crystals. Using HT theory to include contributions from FC factors, FC/HT interferences, and HT coupling, vibronic coupling encoded in polarized UV-absorption spectra at different temperatures was resolved. All modes which were strongly coupled to the lowest energy excitons along the crystalline *a*- or *b*-axis were found to oscillate along their respective axes. By inspecting the absorption spectra at different temperatures, the authors underscored the importance of destructive FC/HT interference at elevated temperatures which may suppress electronic transitions. This work also demonstrated good agreement between experimental spectra and those calculated by considering HT effects, corroborating a relationship between such effects and SF characteristics in crystalline acenes.

Such HT effects have been investigated for hexacene single crystals as well.<sup>57</sup> Using polarized visible-near IR microscopy and calculated spectra, both at different temperatures, dominant HT contributions to spectral features were observed. By using a quasi-harmonic approximation, coefficients of thermal expansion were calculated for individual hexacene unit cells at low and room temperatures through Helmholtz free energy minimization. Density functional theory was then used to obtain phonon modes for each temperature and other calculations were performed to obtain electronic transition dipole moments and their nuclear gradients. Through combining FC factors, FC/HT interference, and HT coupling into HT vibronic theory, complete absorption spectra were calculated for single-crystalline hexacene, which agreed well with the experimental spectra. This work not only solidified the correlation between HT effects and the intricate photophysics for crystalline acenes but provided a theoretical framework by which such correlations can be explored.

To study the impact of molecular symmetry on HT-affected absorption spectra in acenes, considerations have also been made for mono-brominated tetracene, pentacene, and hexacene. This work showed that the loss of symmetry from bromination provided more FC/HT interference thorough vibrational normal modes and increased HT coupling through pairs of such modes. A linear relationship was observed between FC/HT intensity and acene size by projecting the vibrational normal modes to their irreducible representations. Furthermore, the relationship between HT intensity and acene size was found to be quadradic in nature. These calculated correlations aligned with numerical simulations which exhibited an increased agreement with experimental data upon inclusion of HT theory. It was also found that the FC intensity was weaker than FC/HT and HT intensities for the reduced-symmetry species depending on excitation energy, solidifying the need for HT theory in understanding vibronic coupling.

While HT effects impact SF activity in linear acenes, the direct theoretical modeling of the vibronic states of a multi-exciton correlated triplet pair remains challenging due to the desired conservation of its singlet spin state (S=0) beyond the vibrational overlaps. For these reasons, we do not further discuss the theory of HT effects here, and refer the interested reader to work relating such phenomena to vibronic coupling in pentacene and hexacene.<sup>56, 57</sup>

## 5. Anisotropic Singlet Fission in Acene Crystals

In section 5, singlet Davydov splitting and Herzberg-Teller effects were discussed for tetracene, pentacene and hexacene single crystals. In this section, we will focus on anisotropic SF in those polyacene single crystals.

## 6.1 Quantum Decoherence of the Correlated Triplet Pair: Redfield Quantum Dispersion Theory

The process of SF, the generation of two triplet excitons from one following singlet exciton can be described as the chemical reaction in Eq. 1. According to Redfield quantum dispersion theory,  $k_{\rm QD}$  is approximated by<sup>53</sup>

$$k_{\rm QD} \approx \frac{2\lambda\omega_p \Delta E}{\Delta E^2 + \hbar^2 \omega_p^2} \left( \frac{e^{\frac{\Delta E}{k_b T}}}{e^{\frac{\Delta E}{k_b T}} - 1} \right),\tag{17}$$

where  $\Delta E$  is the energy difference between the initial and final states of the QD process,  $\lambda$  is the reorganization energy, and  $\omega_p$  is the system-band coupling energy.  $\hbar$  is the reduced Planks constant,  $k_b$  is Boltzmann's constant, and T is the temperature in Kelvin. If we assume that the decoherence of the correlated pair is strictly the result of vibronic coupling, functional mode analysis can be used to determine  $\omega_p$ . Sun et al. used this method to determine that QD was mostly driven by slow vibrations of  $\omega_p < 50 \text{ cm}^{-1}$  in crystalline hexacene, concluding that the QD was brought about by electron-hole interactions. It was also found that  $\Delta E$  along the a-axis was nearly twice that of  $\Delta E$  along the b-axis. Even though the heterogeneity factor, the ratio of  $k_{\rm QD}$  along the b- and a-axes,  $k_{\rm QD,b}/k_{\rm QD,a}$ , was a variable in calculations but a constant experimentally, the calculated values were well within the range of experimental values.

The coherence of the singlet fission process in acenes has mixed viewpoints. Here, we define coherence as the superposition of two or more states. One such opinion is that the formatin of <sup>1</sup>(TT) from a localized (Frenkel) S<sub>1</sub> is an incoherent process which may contain some charge transfer (CT) character. <sup>102-104</sup> On the other hand, it has been suggested that CT presence can promote the coherent formation of the correlated pair, <sup>105</sup> and has been corroborated for tetracene and pentacene through the observation of nearly coincident formation of both S<sub>1</sub> and <sup>1</sup>(TT) states. <sup>9, 106</sup> Interestingly, Zhu et al. have proposed a mechanism which combines coherent and incoherent processes: the coherent formation of <sup>1</sup>(TT) from S<sub>1</sub> occurs on ultrafast timescales and begins in the excited delocalized S<sub>1</sub>, and the incoherent likeness happens in 180 fs and begins in the localized Frenkel S<sub>1</sub>. <sup>107</sup> However, a more straightforward, and likely appropriate view of the coherent processes is that the S<sub>1</sub> and <sup>1</sup>(TT) states are populated simultaneously and therefore their electronic wavefunctions must be in phase. For the purposes of this review, however, the only coherence which can be stated with certainty is within the correlated triplet pair, and this coherence is what is referred to in this review.

# 6.2 Anisotropic Singlet Fission of Tetracene Single Crystals

As noted above, crystalline tetracene has a triclinic structure with a herringbone arrangement in the *ab*-plane (see Figure 3). Such a structure gives way to anisotropic optoelectronic properties like electron diffusion<sup>60</sup> and polarized optical absorption as shown in section 5. Similar materials have demonstrated anisotropy in excited state exciton behavior due to the polarization of transition dipoles, which is expected to hold true for tetracene.<sup>108</sup> In fact, anisotropic excited states in tetracene were observed by West et al., but not for rubrene.<sup>82</sup> However, transient absorption (TA) spectroscopy has been used by Zhang et al. to address this anisotropy by studying single crystalline tetracene's SF dynamics.<sup>109</sup> Their TA spectra showed a strong anisotropic nature for singlet and triplet excitons depending on probe polarization and are displayed in Figure 6.

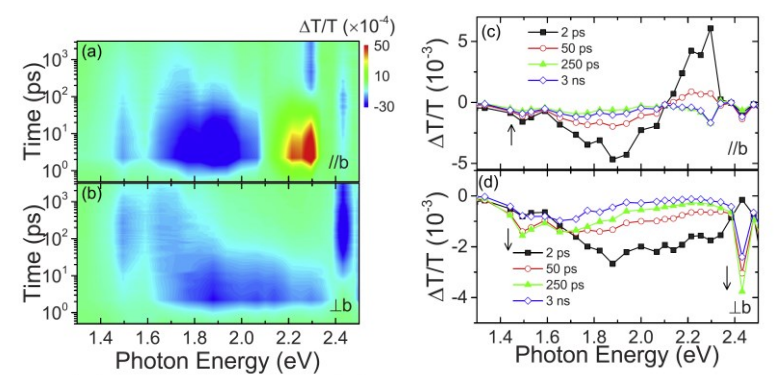


**Figure 6.** Transient absorption (TA) spectra of single crystalline tetracene polarized along (top) and perpendicular to (bottom) the *b*-axis: (a) 2D pseudocolor plots and (b) TA spectra at different time delays.

Reproduced from [B. Zhang, C. Zhang, Y. Xu, R. Wang, B. He, Y. Liu, S. Zhang, X. Wang, and M. Xiao, "Polarization-dependent exciton dynamics in tetracene single crystals," J. Chem. Phys. **141** (2014) 244303.] with the permission of AIP Publishing.

When the tetracene single crystals were probed along the b-axis, three key features were observed as shown in Figure 6(a): ground state bleaching (GSB) between 2.2 and 2.3 eV, photoinduced absorption (PIA) at 1.9 eV, and long-lived PIA at 1.5 eV. However, when probing perpendicular to the b-axis (Figure 6(b)), no GSB was observed, and the PIA modes were clearly different. To further investigate the impact of probe polarization, individual TA spectra and time traces were extracted. Polarized TA spectra at different delays are shown in Figures 6(c) and (d), and time traces at different energies and polarizations are shown in Figures 7(a-f). For the GSB peak, which represents the  $S_0 \rightarrow S_1$  transition, its polarization dependence is owed to the dipole arrangement along the b-axis and is too weak to be observed when probed perpendicular to the b-axis. It was found that the PIA modes may be triggered by excited state absorption (ESA) representing the  $S_1 \rightarrow S_n$  transition whose polarization dependence results from the symmetry of the  $S_1$  and  $S_n$  states. Due to the complexity of  $S_n$  states, the polarization dependence of the ESA and GSB peaks are different, as shown in Figure 7(b). On the other hand, the dynamics of the peak at 1.88 eV are similar along both polarizations.

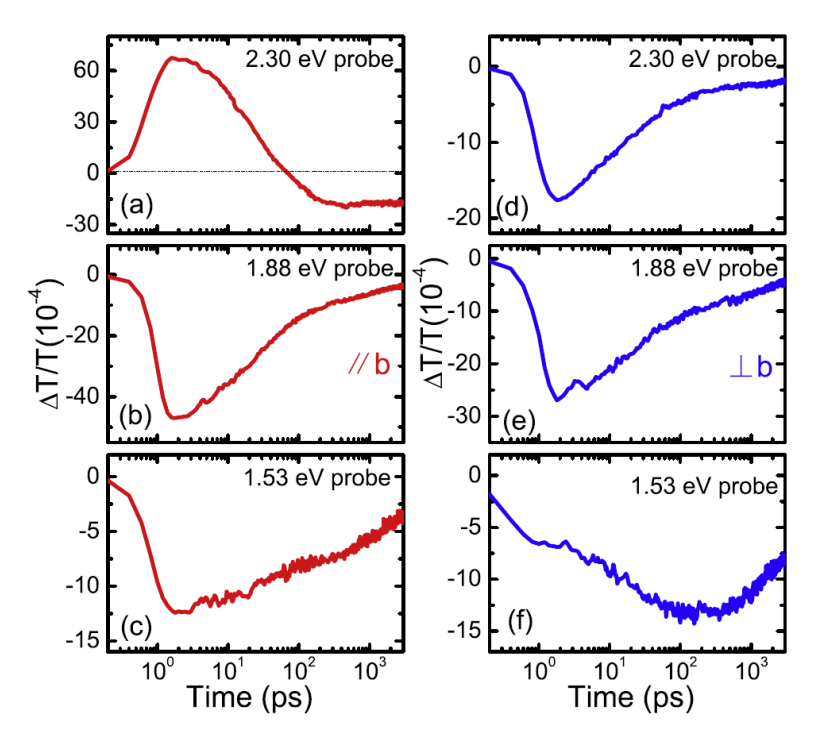


**Figure 7.** Time traces extracted from transient absorption spectra at different energies for single crystalline tetracene probed along (a-c) and perpendicular to (d-f) the crystalline *b*-axis.

Reproduced from [B. Zhang, C. Zhang, Y. Xu, R. Wang, B. He, Y. Liu, S. Zhang, X. Wang, and M. Xiao, "Polarization-dependent exciton dynamics in tetracene single crystals," J. Chem. Phys. **141** (2014) 244303.] with the permission of AIP Publishing.

The long-lived PIA feature at 1.53 eV has been ascribed to the triplet state, and its instantaneous rise and following delayed rise components are attributed to the transition from  $S_1$  to  $S_n$  states, respectively. The polarization-dependence of the transient data align well with previous assertions of the PIA feature containing both singlet and triplet contributions. Furthermore, PIA at 1.53 eV observed from polycrystalline tetracene was much weaker than that of the single crystal sample. This is due to differences in dipole alignments between the  $S_1 \rightarrow S_n$  and  $T_1 \rightarrow T_n$  which causes their contributions to the ESA feature to be different as well.

By thoroughly investigating the polarized TA data from tetracene single crystals, Zhang et al. could understand correlations between singlet and triplet populations. <sup>109</sup> In fact, they were able to reconstruct the triplet dynamics by eliminating the singlet contributions to the PIA at 1.53 eV following Wilson's approach. <sup>111</sup> This showed that dynamical behaviors for both polarizations were similar, excluding amplitude, and the polarization ratios did not change much over time. It was also found that the reconstructed triplet signal was proportional to the total density of triplet excitons, and that the time constant of the SF process was slightly above previously reported values.

Birech et al. also used polarized TA to study the ultrafast excitation dynamics of single crystalline tetracene around the same time.<sup>69</sup> Using optically thin tetracene single crystals, they found that the fission process can happen in different mechanisms which occur on different timescales, aided by deconvoluting the TA spectra. It was shown that ultrafast fission channels from the higher Davydov state, which lies perpendicular to the *b*-axis, could be identified. Furthermore, the authors demonstrated that vibrationally excited singlet states, which are suppressed when pumped along the *b*-axis, could be identified as well.

Birech et al. also showed that DS occurred at room temperature for tetracene single crystals in the  $T_1 \rightarrow T_n$  transitions with a value of 0.04 eV.<sup>113</sup>

Recently, Wang et al. reported polarized two-dimensional electronic spectroscopy (2D-ES) measurements on single crystalline tetracene where the method was used to study SF dynamics specifically in the excited state. 114 This method allowed the authors to probe sub-picosecond dynamics and vibrational coherences which were determined to be very sensitive to photoexcited states. Their analysis also suggested that the observed high-frequency mode was coupled to the locally excited and correlated triplet pair states which may contribute to energy compensation. This work highlighted the importance of the relationship between exciton/vibration coupling and dipole-dipole interactions in endothermic SF molecular systems.

Comparisons of polycrystalline and single-crystal species of tetracene have also been conducted by Beardeen et al regarding the material's photophysical characteristics. <sup>7, 115</sup> The authors observed a faster decay rate of the singlet state in polycrystalline tetracene compared to single-crystal samples, as well as a reduced temperature dependence on the rate. <sup>115</sup> To further examinine the impact of sample structure on SF in tetracene, the polycrystalline samples were annealed, which resulted in larger crystalline domains that caused the material to behave more like a single-crystalline sample. These results could also provide some explanation to observed differences in SF rate in tetracene, ranging from 250 to 300 ps. It was hypothesized that diffusion of excitions to defect and interface states in polycrystalline tetracene contributed to the accelerated SF rate. SF of different polymorphs of polycrystalline tetracene has also been investigated by Arias et al, showing an acceleration of SF with increasing crystal size, depending on the polymorph. <sup>116</sup> These works highlight the effects of sample morphology and molecular packing on the SF characteristics of tetracene materials.

## 6.3 Anisotropic Singlet Fission of Pentacene Single Crystals

Pentacene has been studied extensively as a SF material and is often used as a benchmark for other systems. 9-11, 54, 65, 75, 117-122 However, most ultrafast experiments have been conducted on polycrystalline pentacene due to the challenges associated with growing a macroscopic single crystalline sample. In 2014, Kolata et al. used ultrafast pump-probe spectroscopy to study SF dynamics in single crystalline perfluoropentacene (PFP). 123 For this model system, they demonstrated that anisotropy in the material's SF character produces different relaxation mechanisms for different crystal orientations thereby impacting conversion efficiency. Figures 8(a-b) show the crystal structure for PFP which exhibits anisotropic packing in the *bc*-plane, a slip-stacked structure along the *b*-axis, and a herringbone pattern along its *c*-axis. Such an arrangement minimizes interactions between molecules in the face-to-edge direction which only leaves interactions along the *b*-axis for contributions to SF. This is manifested in the observed anisotropy in the linear absorption spectra for PFP shown in Figures 8(c-e). The spectra along the *b*- and *c*-axes, show an absorption maximum near 1.7-1.8 eV which is ascribed to the singlet state based off the nearby maximum for the sample in solution. This anisotropy is made even more apparent by the time-resolved differential absorption spectra along the different crystal axes shown in Figures 8(f-h).

Another pentacene derivative, 6,13- bis(triisopropylsilylethynyl)pentacene (TIPS-pentacene) has also been investigated using polarized TA microscopy to better understand its SF dynamics. <sup>124</sup> Using a white light probe with tunable polarization, the authors were able to investigate the anisotropic nature of SF in this single-crystalline material. It was shown that the correlated triplet pair remained intact for hundreds of picoseconds before dissociating which was caused by triplet-triplet interactions stemming from the stacking of  $\pi$ -orbitals. This work used ultrafast techniques to uncover connections between structure and SF dynamics, promoting  $\pi$ -stacking as a favorable structure when designing SF systems.

TIPS-pentacene single crystals have also been studied using 2D white-light (2D-WL) and TA microscopies by Jones et al..<sup>125</sup> It was found that low-energy singlet states were dispersed throughout the

microcrystals with higher densities near the material's edges and defects. They also showed that the spectra were indicative of the slip-stacked geometry which enhanced CT coupling. Interestingly, the picosecond kinetics of the low-energy singlet states were similar to those for the  $^1(T_1T_1)$  which indicated that these sites were the location for internal conversion. Combined, the 2D-WL and TA imaging were used to provide population geometry and spatial mapping, respectively. A correlation was found between the crystal edges, interfaces, and defects with the observed low-energy states, and it was determined that the singlet energies resulting from the molecular geometry provided a mechanism for resonant energy conversion between singlet and triplet populations.

Looking intitially at the first singlet resonance, the authors observed bleaching along both b- and c-axes shortly after excitation. PIA was observed along the b-axis and was indicative of partially delocalized excitations between two molecules. Photoinduced luminescence (PIL) was also observed at a lower energy which is typically ascribed to the sharing of excitations between neighboring molecules. Investigating the dynamics along the a-axis revealed intense PIA at 2.28 eV which was deemed the dipole-allowed  $T_1 \rightarrow T_4$  transition. The change in lineshape from asymmetric to symmetric with time was determined to be a result of dephasing of the correlated triplet pair. The dynamics of the rise of the  $S_1$  resonance's GSB and PIA along the a-axis, which are associated with the correlated triplet pair, happen at the same time which suggests that the triplet pair is immediately formed upon excitation, before the population of excimer-like states below the  $S_1$  state. The authors used a rate equation model to quantify these dynamics and found excellent agreement with simulations. They concluded that the partially delocalized triplets along the b-axis were correlated with the stacking geometry, that the dephasing of the correlated pair is observed in the asymmetry of the dynamics along the a-axis, and that one third of the correlated pairs separate on the order

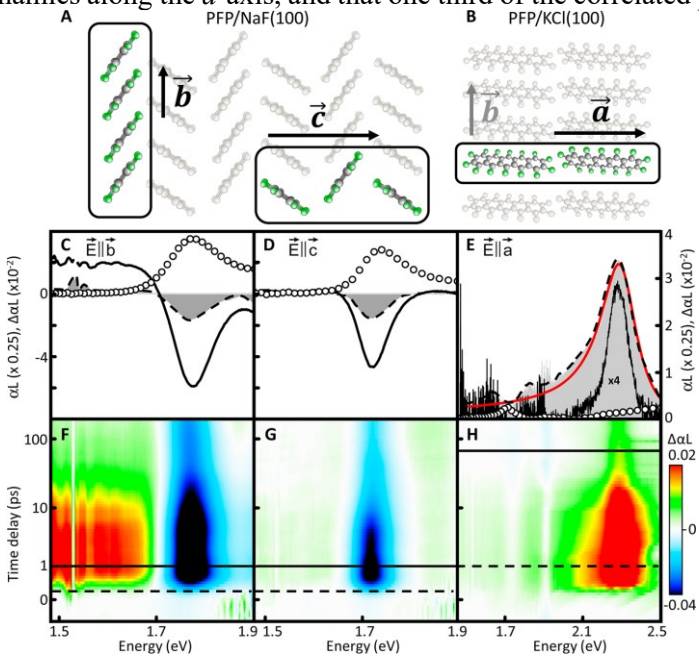


**Figure 8.** Crystal structure perfluoropentacene (PFP) in the (A) bc- and (B) ab-planes. Absorption of PFP along the (C) b-, (D) c-, and (E) a-axes: linear absorption (open circles), transient absorption (TA) after time delays of 300 fs (dashed) and 1 ps (solid) for the b- and c-axes. Dashed and solid lines correspond to 1 and 90 ps delay along the a-axis. 2D pseudocolor plots of TA spectra along the (F) b-, (G) c-, and (H) a-axes. Reproduced with permission from ACS Nano **8** (2014) 7377. Copyright 2014, American Chemical

Society.

of nanoseconds.

More recently, Deng et al. used polarized TA microscopy along with *ab initio* simulations to study the impacts of vibronic coupling on SF in single crystalline pentacene.<sup>54</sup> They found that SF was facilitated by a vibrational coherence of 35.0 cm<sup>-1</sup> which persists for picoseconds. This phonon was found to be facilitated by a cross-axial CT intermediate state and is the driving force for the QD of correlated triplet pairs.

For the TA experiments, the pump was polarized along the b-axis of the pentacene single crystal sample while the pump was polarized along either the a- or b-axis. These time- and angle-resolved differential transmission spectra are shown in Figures 9(a) and (c), where GSB and PIA have positive and negative magnitudes, respectively. The triplet PIA bands exhibit clear anisotropy in Figures 9(b) and (d), and suggests the coexistence of two different types of correlated triplet pairs:  ${}^{1}(T_{1}T_{1})_{bb}$  probed along the b-axis, and  ${}^{1}(T_{1}T_{1})_{aa}$ , probed along the a-axis. It was found that the  ${}^{1}(T_{1}T_{1})_{aa}$  triplet pair was 30meV more

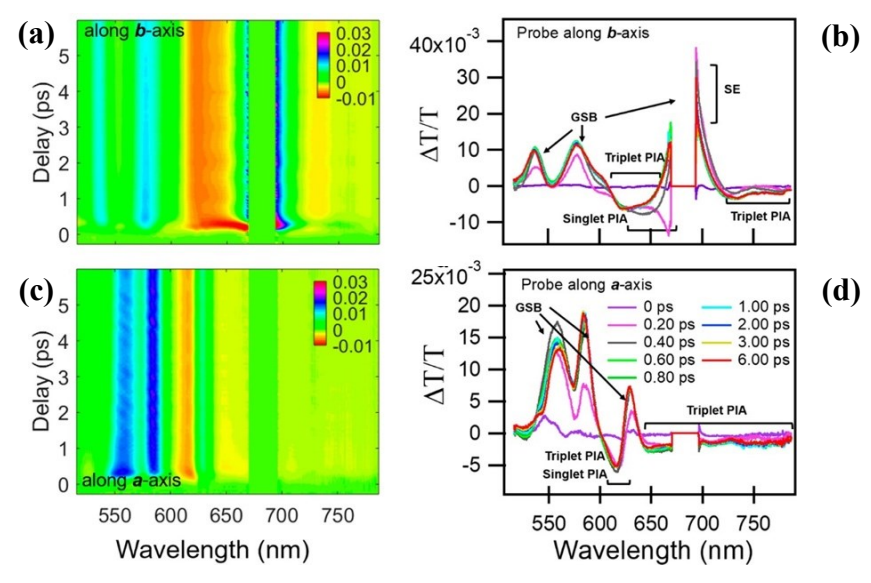


**Figure 9.** Polarized transient absorption (TA) spectra of single-crystalline pentacene: 2D pseudocolor plots probed along the (a) *b*-and (c) *a*-axes, TA spectra at different time delays probed along the (b) *b*- and (d) *c*-axes.

Reproduced with permission from J. Phys. Chem. Lett. 12 3142(2021).). Copyright 2021, American Chemical Society.

thermodynamically stable than the  ${}^{1}(T_{1}T_{1})_{bb}$  variety, which agreed with calculations. Furthermore, this study reveals notable triplet DS in pentacene through the TA microscopy experiments.

Close inspection of the TA spectra revealed oscillatory features in the triplet PIA modes with progressing time, as shown in the time traces for the two polarizations in Figure 10(a). The authors

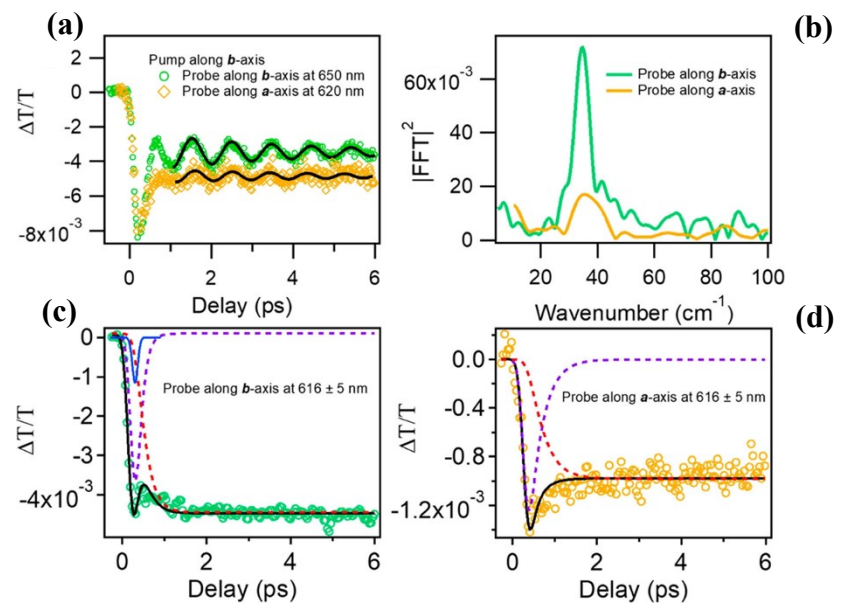


**Figure 10.** (a) Time traces from transient absorption measurements of single-crystalline pentacene probed along the *a*- and *b*-axes exhibiting oscillations, (b) Fourier-transformations of oscillations from (a) along the *a*- and *b*-axes, time traces after deconvolution of oscillations probed along the (c) *b*- and (d) *a*-axes.

Reproduced with permission from J. Phys. Chem. Lett. 12 3142(2021).). Copyright 2021, American Chemical Society.

performed a Fourier transform on the time traces which revealed a dominant frequency of  $34.5 \text{ cm}^{-1}$  when probed along either crystal axis, as shown in Figure 10(b). This feature was attributed to coherent phonons which accompanied photogenerated excitons. Fittings of the time traces allowed the authors to investigate both  $k_{\rm F}$  and  $k_{\rm QD}$ , as shown in Figures 10(c) and (d). When probed along the *b*-axis, it was found that the generation of the correlated triplet pair and its subsequent quantum decoherence had rate constants of 8.1 and 5.7 ps<sup>-1</sup>, respectively. Additionally, the formation rate when probed along the *a*-axis was 1.5 times slower than in the perpendicular direction while the QD rates were comparable. Since the rates of QD were comparable to the pair's formation, it was concluded that both processes are of about equal importance in pentacene single crystals. The authors then went on to calculate the QD rate constant by assuming that the process is mainly driven by vibronic coupling between  $^{1}(T_{1}T_{1})$  and the surrounding heat bath using Redfield dispersion theory. Interestingly, they found that the QD process was driven by slow vibrational modes (<100 cm<sup>-1</sup>) with no notable directionally with respect to the crystal axes.

Overall, the authors connected their results in the conclusion that the SF mechanism for pentacene single crystals was coherent and facilitated by a cross-axis charge transfer state  $(CT_{ab})$  and the coherent phonon described above. It was found that  $CT_{ab}$  is nearly degenerate with  ${}^{1}(T_{1}T_{1})_{aa}$  as well as  ${}^{1}(T_{1}T_{1})_{bb}$ , making it ideal to mediate the process. Functional mode SF theory corroborated that the process was made possible through the coherent phonon and that it contributed greatly to and from the CT intermediate. The  $CT_{ab}$  state encompasses the cross-axial collective motion of neighboring pentacene molecules. The authors suggest that the process is more dominant along the b-axis than along the a-axis, which aligns with the differences in intensity for the peaks shown in Figure 10(b) along with calculations presented in the original

paper. Although these calculations presented other FC-active phonons, only the phonon of 35.0 cm<sup>-1</sup> was experimentally observable.

The presence of a coherent phonon reported by Deng et al. was corroborated by Seiler et al. using femtosecond electron diffraction. With assistance from density functional theory and molecular dynamics simulations, they suggest that coherent and incoherent movements contribute to SF in pentacene single crystals. The simulations uncovered atomic and coherent phonon movements which agreed with their experimental data, and noted the significance of the role of long-range intermolecular structural dynamics for the accurate description of SF in pentacene, considering processes which have effects outside of the unit cell.

Stimulated Raman spectroscopy has also been used to investigate the SF character of single-crystalline pentacene. Hart et al. found that energy shifts in pairs of excited state peaks relative to the ground state denoted the creation of an intermediate state.<sup>65</sup> In this process, a 1369 cm<sup>-1</sup> ground state peak divides into two peaks; one at 1365 cm<sup>-1</sup> and the other at 1382 cm<sup>-1</sup>, as shown in Figure 11(a). After 1 ps, the two peaks shift to lower and higher frequencies, respectively, as shown in Figure 11(b). It was proposed that this process was the result of the formation of both cationic and anionic species from partial intermolecular electron density transfer. Extracting the time traces from the collected stimulated Raman spectra, the authors were able to evaluate the dynamics of the CT intermediate (1365 cm<sup>-1</sup>) and the triplet transition from its absorption at 840 nm with ultrafast resolution. The evolution from the CT state to the triplet state around 500 fs is clear. Additionally, the calculated frequencies for the neutral, cationic, and anionic species are shown in Figure 11(c), which agreed qualitatively with the authors' experimental results. This work demonstrated the usefulness of ultrafast time-resolved vibrational spectroscopy in contributing to our deeper understanding of SF processes. Further, the authors highlighted considerations that must be taken when working with polycrystalline or single crystal samples: polycrystalline systems contain more defects, have crystal lattice interfaces, and are not eligible for studies based on crystal lattice orientation. Such differences complicate the interpretation of experimental results through modeling and lead to misinterpretations.

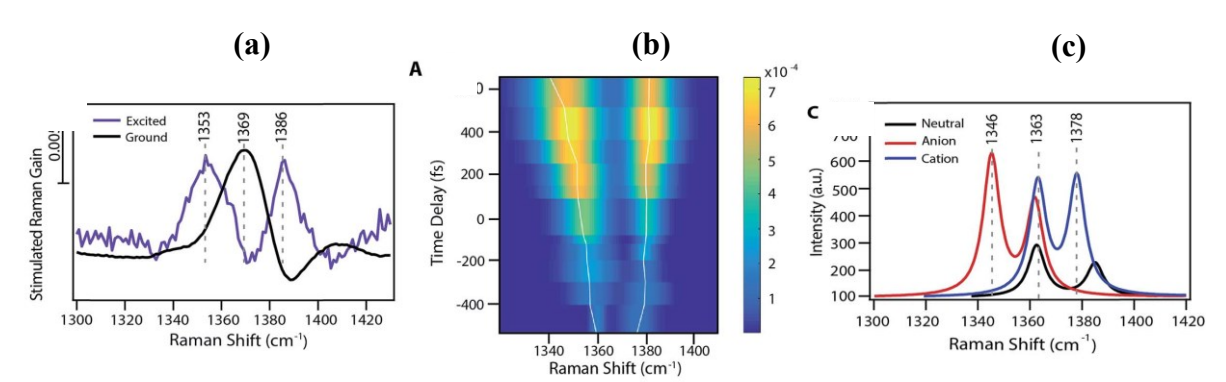


**Figure 11.** (a) Ground and excited state Raman spectra of single-crystalline pentacene showing splitting of the ground state peak, (b) divergence of excited state peak position over time, and (c) calculated Raman spectra for the neutral, anionic, and cationic species in single crystalline pentacene

Reproduced with permission from Chem. Sci. 9 (2018) 1242. Copyright 2018 Royal Society of Chemistry.

Recent developments like ultrafast interferometry-based pump-probe microscopy techniques have also been used to study SF in pentacene thin films. These techniques have revealed clear anisotropy along different crystal directions and have provided insights into the dynamics of singlet excitations and correlated pair formations. These findings further underline the anisotropic nature of SF.

## 6.4 Anisotropic Singlet Fission of Hexacene Single Crystals

The analysis of the optoelectronic properties of single crystalline larger polyacenes such as hexacene has been challenging largely due to lacking sufficient preparation techniques. Busby et al. experimentally studied the SF dynamics of hexacene thin films in 2014, where TA measurements observed that SF occurred on the order of 500 fs. <sup>84</sup> This rate is much faster than smaller acenes, with SF in tetracene ranging from 10 to 100 ps, <sup>111, 128, 131</sup> but yet much slower than pentacene whose SF process occurs in around 100 fs. <sup>9, 75, 117, 118</sup> The intermediate SF rate of hexacene was explained by a multiphonon relaxation process which was accompanied by a significant exotherm. <sup>84</sup> More recently, Sun et al observed significant anisotropicy in the SF character of single crystalline hexacene using polarized TA microscopy. <sup>53</sup> They found that while the  ${}^{1}(T_{1}T_{1})$  forms at comparable rates along the a- and b-axes, the subsequent QD rates exhibited anisotropy.

The TA spectra were collected from the single crystalline hexacene samples along a- and b-axes while the sample was pumped along its b-axis. The differential transmission ( $\Delta T/T$ ) pseudocolor plots from probing along the b-axis are shown in Figures 12(a) and (b) while those from probing along the a-axis are shown in figures 12(c) and (d). Spectra at different time delays are shown in Figures 12(e) and (f) for probing along the b- or a-axes. Along either crystal axis, positive features were observed between 620 and 730 nm which were attributed to GSB and the following recovery. On the other hand, negative features below 620 nm were indicative of PIA from the  $T_1 \to T_n$  transitions. Further inspection revealed that the broad features from 496 to 577 nm were short-lived and were due to ESA from the  $S_1 \to S_n$  transition. The

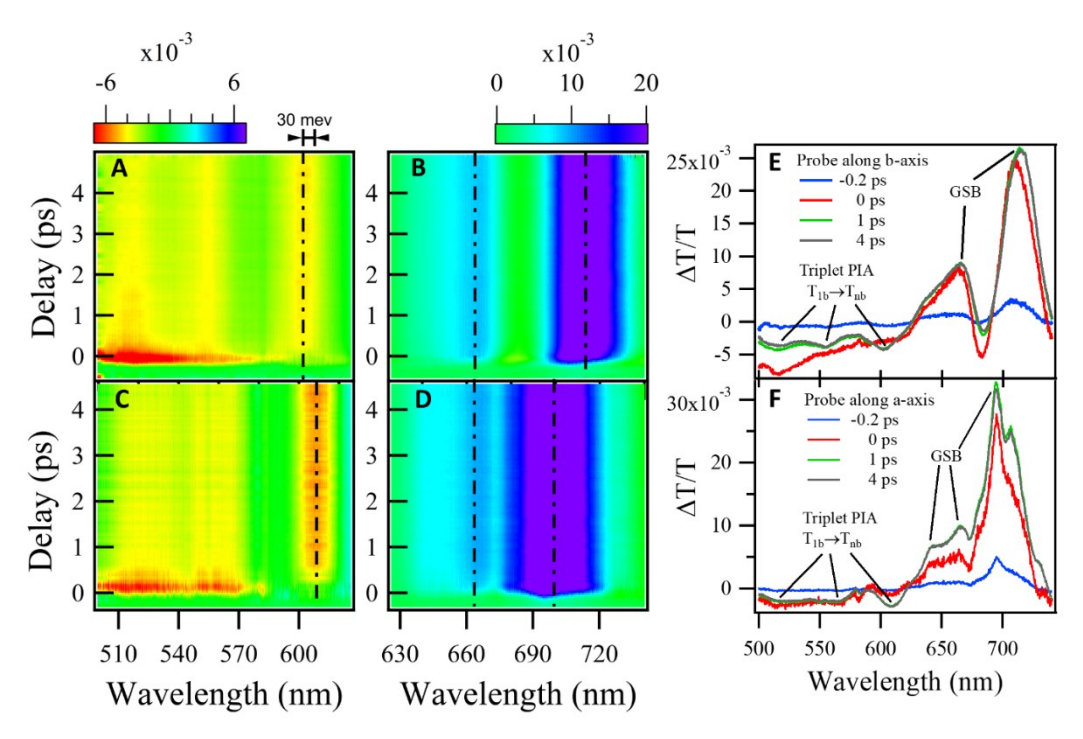


**Figure 12.** Transient absorption (TA) spectra of single-crystalline hexacene: 2D pseudocolor plots of TA spectra probed (a & b) along the *b*-axis and (c & d) along the *a*-axis; TA spectra at different time delays probed (e) along the *b*-axis and (f) along the *a*-axis.

Reproduced with permission from iScience 19 (2019) 1079. Copyright 2019 Elsevier.

peaks from 508 to 544 nm and from 590 to 620 nm persisted for a longer time and were labeled as triplet transitions. The authors observed anisotropy in the triplet transitions shown in Figures 13(a) and (c) where a 9 nm redshift was noted between the peaks at 599 and 608 nm which were collected along the *b*- and *a*-

axis, respectively. Such a property indicated that the triplet excitons observed along the different crystal axes were unique from one another with a DS energy of 30 meV where the  $T_{1b} + T_{1b}$  species was more energetically stable than the  $T_{1a} + T_{1a}$ .

Kinetic traces were extracted from the polarized TA spectra at different wavelengths to investigate the rates of SF in single crystalline hexacene. Global fittings of the kinetic traces in Figures 13(a) and (b) revealed that the formation rates along both axes were comparable with  $k_{F,bb} = 4.5 \text{ ps}^{-1}$  and  $k_{F,aa} = 5.0 \text{ ps}^{-1}$ . On the other hand, the rate constants for QD along the different hexacene axes were remarkably different with  $k_{QD,bb} = 6.7 \text{ ps}^{-1}$  and  $k_{QD,aa} = 3.3 \text{ ps}^{-1}$ , revealing the anisotropic nature of SF in single crystalline hexacene.

Considering the observed DS character, isotropic  ${}^1(T_1T_1)$  formation, and anisotropic QD, the authors then developed a unified vibronic model of the SF process. This model used a non-adiabatic functional mode approach. <sup>132, 133</sup> It was determined that the SF process was primarily controlled by the QD rate rather than that of formation. The anisotropy of the correlated triplet pair state was found to be caused by the anisotropic environment in the single crystal samples. It was also found that the QD process in hexacene was driven only by vibronic coupling between the  ${}^1(T_1T_1)$  state and low-frequency phonon modes. The calculations also confirmed that the  $T_{1b} + T_{1b}$  was at a lower energy level than the  $T_{1a} + T_{1a}$  which is contradictory to tetracene and pentacene.

The recent studies into anisotropic SF in polyacenes provides valuable information for the design of organic semiconductors and photonic devices which can be applicable to other organic systems. Furthermore, the insights gained into the necessary instrumentation for studying SF and optoelectronic properties in organic semiconductors will aid in the design and investigation into new, more efficient systems. Specifically, these methods can be used to study the photophysics which govern and are governed by oriented transition dipoles in other molecular crystals.

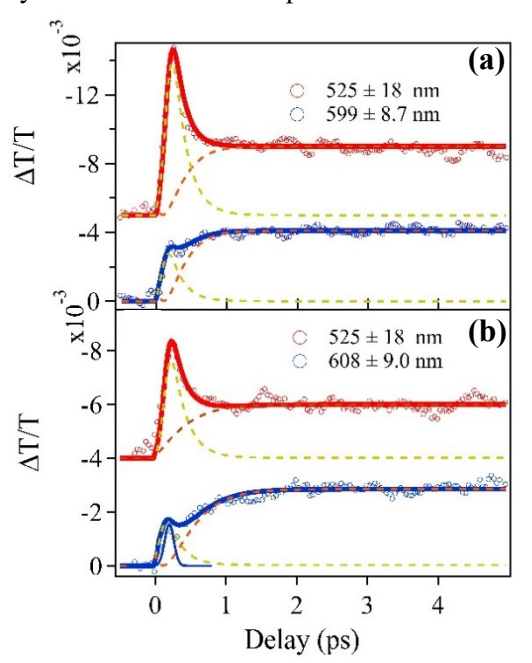


**Figure 13.** Time traces extracted from transient absorption spectra of single crystalline hexacene at different energies probed (a) along the *b*-axis and (b) along the *a*-axis.

Reproduced with permission from iScience **19** (2019) 1079. Copyright 2019 Elsevier.

In addition, rubrene, a derivative of tetracene, has been studied extensively 134-139 and single crystalline rubrene has exhibited fast and efficient SF. 137, 138 However, outstanding challenges and questions remain regarding the SF mechanism for this polyacene. For example, the impact of molecular packing and intermolecular interactions is not explicit, due in part to a lack of focus on the anisotropic nature of SF in

rubrene. Here we consider some important advancements in the understanding of SF in rubrene single crystals. Using ultrafast transient transmittance and 2D-ES methods as well as theoretical modeling, the SF mechanism for single-crystalline rubrene was mapped up to the spin dephasing step. 140 The dynamical features from these observations also exhibited anisotropic characters. In addition to observing an increased rate along the herringbone axis compared to the slip-packed axis, a fast component of ~100 fs was observed in both directions. This difference was attributed to delocalization of the  $S_1$  excitons, vibronic couplings, and coupling to the correlated triplet pair. More recently, Liu studied the effects of different stacking geometries on SF in single crystalline rubrene using ultrafast TA microscopy. 141 They observed coherent and incoherent SF pathways in orthorhombic and triclinic morphologies because of tighter  $\pi$ - $\pi$  stacking. On the other hand, the monoclinic moiety with looser packing only exhibited incoherent SF channels. Furthermore, it was observed that incoherent SF in orthorhombic rubrene crystals was thermally activated while it was more spontaneous for monoclinic and triclinic samples. Using quantum-mechanical calculations, the authors confirmed that electronic coupling strength was the culprit for the difference in SF dynamics among the different crystal arrangements. Even without a focus on the anisotropic nature of SF in this investigation, it was made clear that molecular packing and orientation in rubrene single crystals affects their SF pathways and should be considered when designing devices using organic crystal semiconductors.

## 6.5 Morphology Effects on Optoelectronic Properties in Other Materials.

Organic semiconductors other than polyacenes have also been investigated for their photo-physical properties which can be affected by morphology brought about by functionalization. 142-146 For example, different functionalizations of fluorinated anthradithiophene (FADT) have been studied using absorption, photoluminescence, and density functional theory and revealed dynamics of CT, correlated triplet pairs, and Frenkel excitons in solution and single-crystalline samples. 142 For the solution samples, the authors observed an FC state at all presented concentrations and an excimer state for higher concentrations. In single crystalline FADT samples, absorption, emission, and calculations led to the discovery of mixing between Frenkel and CT excitons and that the degree of mixing was dependent on crystal geometry. Emission studies of the functionalized FADT single crystals identified Frenkel excitons, correlated triplet pairs, and selftrapped excitons. A twisted column arrangement resulted in Frenkel exciton formation over a range of temperatures with the appearance of  ${}^{1}(T_{1}T_{1})$  and self-trapped states at lower temperatures. On the other hand, the "brickwork" arrangement exhibited all three exciton types across the whole temperature range. Interestingly, the sandwiched-herringbone geometry did not exhibit correlated triplet pair features, although Frenkel and self-trapped species were apparent at all temperatures. This work demonstrated the severe impact that crystal structure can have on the optoelectronic properties of a material, especially for organic semiconductors.

The effects of molecular packing in single-crystalline FADT SF have also been investigated by polarized TA microscopy. It was found that while "brickwork" and twisted column structures were probed along their CT axis the population of the  $^1(T_1T_1)$  state could be observed on the ps timescale, and when probing normal to the CT axis a decrease in singlet state population was observed. It was found that the ratio of the conversion rate relative to that of exciton self-trapping was up to 100% depending on crystal structure. The authors also found that a sandwiched-herringbone structure only featured a reduction in self trapping and singlet states, suggesting that SF is prohibited by the lower symmetry of the structure. This was quantified by the 3x increase in energy difference between the  $S_1$  and CT states for the sandwiched-herringbone structure compared to the other morphologies. This work further exemplified the impact of molecular ordering on optoelectronic properties for organic semiconductors and provided quantitative information useful for designer semiconductor materials. Although single-crystalline samples offer quantification of anisotropic effects and more straightforward theoretical analyses, polycrystalline organic semiconductors offer easier and more cost-effective production.

Another SF material that has been investigated for uses in photovoltaics is perylene-3,4:9,10-bis(dicarboximide) (PDI). <sup>148-152</sup> Using absorption and emission techniques, the effects of derivatizing PDI molecules to change molecular arrangements were investigated for polycrystalline thin films of PDI and TIPS-pentacene. <sup>150</sup> In this film, it was determined that after SF occurred in TIPS-pentacene to form a triplet, a PDI/TIPS-pentacene geminate radical ion state was formed which led to intersystem crossing, and charge recombination that also produced the triplet TIPS-pentacene state. This work highlighted the importance of understanding all pathways which can lead to exciton formation in organic semiconductors. The SF characteristics of a PDI derivative have also been investigated in polycrystalline thin films. <sup>148</sup> TA measurements of the sample discovered that although SF was quite slow (a few nanoseconds), its triplet conversion efficiency was high (about 50%). This work added another potential material to the growing list of organic semiconductors that exhibit SF properties.

#### 7. Anisotropic Triplet Diffusion in Polyacene Crystals

Exciton diffusion, the process of transporting energy in a material via the movement of an exciton, dictates the performance of many processes from photosynthesis to optoelectronic devices. <sup>153-156</sup> It has been found that long-range order in materials promotes exciton diffusion. <sup>157, 158</sup> Exciton diffusion has also been shown to be anisotropic in organic crystals, but such interpretation is not straightforward. <sup>159, 160</sup> Recent valuable information into exciton diffusion has been provided by way of spatial, temporal, and spectral analyses. For example, Wan et al. have identified a cooperative singlet/triplet transport pathways in tetracene. <sup>59</sup> A study by Akselrod et al. determined that instead of photon emission and reabsorption being the main mode of exciton transport in crystalline tetracene, energy is transported by an electron hopping mechanism. <sup>60</sup> A better understanding of anisotropic exciton diffusion in molecular crystals may aid in the design of more efficient organic photovoltaics by directionally optimizing the process.

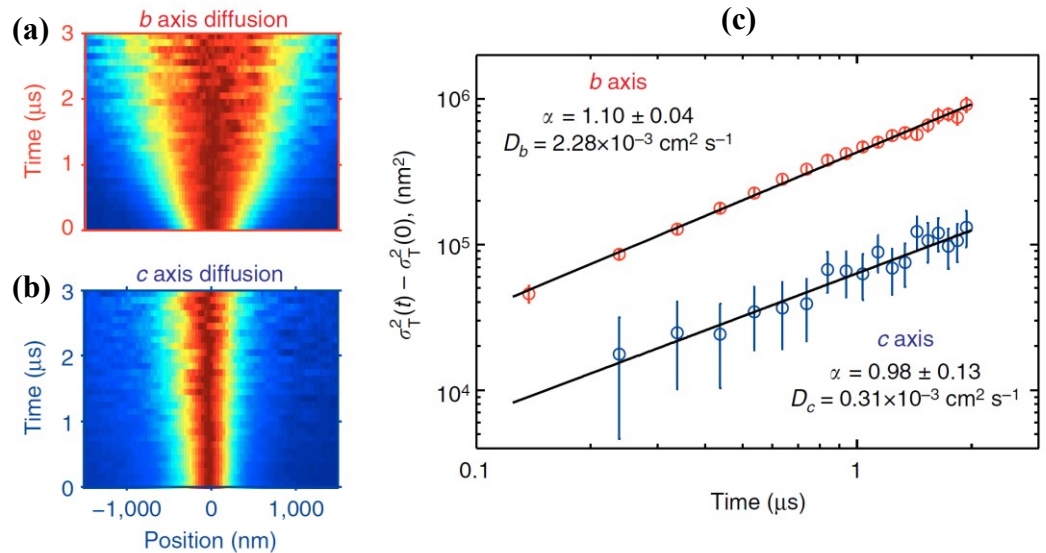


**Figure 14.** Fluorescence microscopy of triplet diffusion along the (a) *b*- and (b) *c*-axes; comparison of anisotropic diffusion rates (c).

(G. M. Akselrod et al., Nat. Commun. 5 3646(2014).

In molecular solids, excitons are believed to be transported by the "random walk" process in which localized excitement is transferred to nearby molecules.  $^{161, 162}$  In the random walk mechanism, exciton spin state dictates the type of hopping that occurs: singlet excitons undergo Förster energy transfer which is a dipole-dipole interaction with a distance of about a few nanometers, as interaction decays proportionally to  $R^{-6}$  where R is radius.  $^{163}$  Triplet excitons, on the other hand, use Dexter energy transfer which

simultaneously exchanges two electrons between neighboring molecules which avoids any spin-forbidden transitions to the ground state. <sup>162, 164, 165</sup> Dexter energy transfer depends on the spatial and temporal overlap of the molecular wavefunctions of neighboring molecules to facilitate the process. In materials like polyacenes, triplet excitons are dominant because of SF. In this section we will focus on anisotropic triplet exciton diffusion in single crystalline tetracene, pentacene, and hexacene.

In tetracene crystals, the molecules are arranged in a herringbone pattern that results in a greater overlap of p-orbitals in the crystal's ab-plane than along the c-axis, as shown in Figure 3. the asymmetry in orbital overlap results in significant anisotropy in Dexter transfer rates, thereby resulting in anisotropic exciton diffusion. 162 To date, this anisotropic exciton diffusion has been theoretically predicted 162 and experimentally observed in the steady state of rubrene single crystals. 166 Work by Akselrod et al. investigated possible differences between triplet diffusion in crystalline tetracene. in the ab-plane versus along the c-axis and reported notable anisotropy. 60 Using fluorescence microscopy, they were able to map exciton diffusion in space and time along both b- and c- crystal axes, as shown in Figures 14 (a-c). A sevenfold anisotropy was observed between the b- and c-axes, which was consistent with previous theoretical predictions. 162 Because exciton transport in tetracene depends on wavefunction overlap, previous measurements of exciton transport along the c-axis have displayed wide variations. In tetracene, unlike other conjugated organics, the dipole moment is perpendicular to the long molecular axis. From the orientation of the dipole moment, the highest reabsorption rate caused by the strongest dipole alignment occurs along the b- and c-axes. This results in the highest anisotropy in reabsorption to be between the aand b-axes with the anisotropy between the b- and c-axes being smaller. This assessment aligns with the three-fold anisotropy in absorption and emission between the a- and b-axes reported previously. 167 However, triplet exciton diffusion relies on  $\pi$ -orbital overlap. Therefore, the largest anisotropy in triplet exciton hopping should be between the b- and c-axes. Akselrod et al. determined that the observed distribution broadening was the result of triplet hopping instead of reabsorption but noted that small contributions from radiative transfer cannot be overlooked. However, the anisotropy in exciton diffusion between the a- and b-axes was not discussed.

TA imaging has also been used to determine the effects of SF driving forces on exciton diffusion in single crystalline tetracene, rubrene, and TIPS-pentacene. It was found that while rubrene and TIPS-pentacene exhibit the fastest exciton diffusion along the a-axis, the fast exciton transport in tetracene happened along the b-axis, as shown in the TA microscopy images in Figures 15(a-c).

By calculating the modified contribution to triplet transport, the authors found that the difference in SF endothermicity between TIPS-pentacene, rubrene, and tetracene produces prominent singlet-mediated SF pathways. <sup>168</sup> In crystalline tetracene, the contribution of these pathways is 21x greater than the contribution from triplets alone. On the other hand, the ratios of singlet-to-triplet contributions are 7 for rubrene and 0.6 for TIPS-pentacene. This results in the effective triplet transport lengths being hundreds of nanometers in nanoseconds for tetracene and rubrene. This TA microscopy study on anisotropic exciton diffusion in crystalline acenes demonstrated that singlet-mediated diffusion pathways can impact triplet transport on the ps and ns timescales. As such tetracene and similar molecular crystals like rubrene are ideal for utilizing SF in double-layer photovoltaics because the SF and triplet transport directions can be optimized.

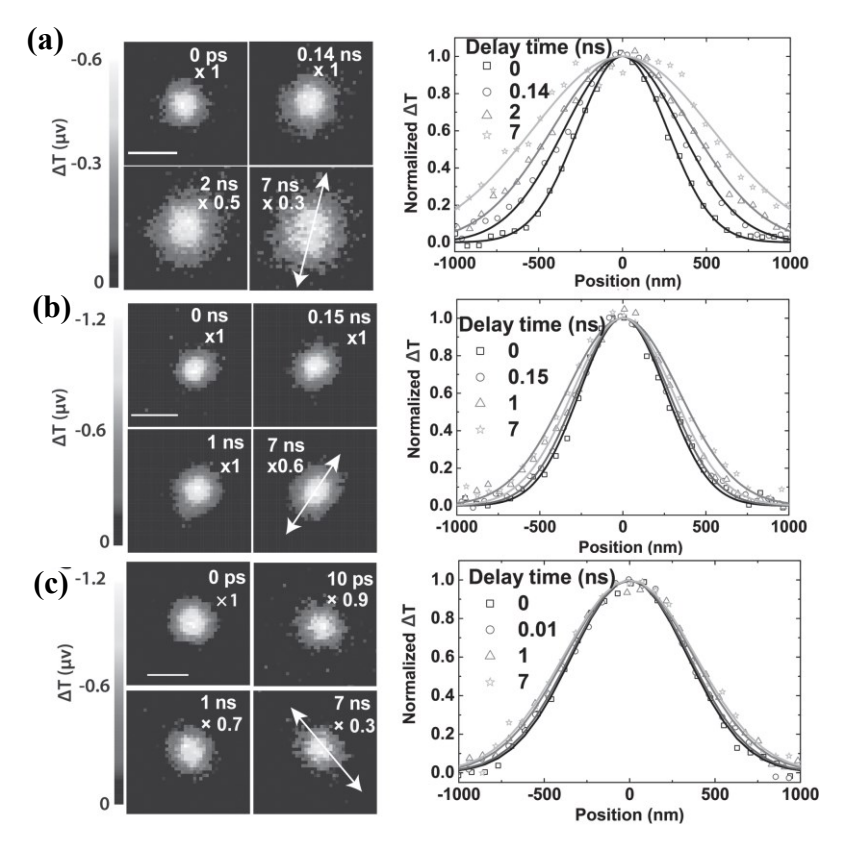


**Figure 15.** Transient absorption microscopy images (left) and diffusion plots (right) for (a) tetracene, (b) rubrene, and (c) TIPS-pentacene single crystals. Images were taken in the *ab*-plane and plots follow arrows indicated in images.

Reproduced with permission from Adv. Mater. 28 7539(2016). Copyright 2016, John Wiley & Sons.

Ultrafast polarized TA microscopy has provided the direct observation and visualization of exciton diffusion in single-crystalline tetracene with 200 fs time resolution and 50 nm spatial resolution.<sup>59</sup> By looking at the TA images at different pump-probe delay times, the progression of the triplet exciton diffusion can be seen in Figure 16(a). The change in transmission with respect to pump-probe distance are shown explicitly along the *b*- and *a*-axes in Figures 16(b) and (c). The progression of the transport results in the TAM image become ellipsoidal and fitting the data with a 2D surface function allowed the authors to determine the fast and slow transport axes, demonstrating anisotropic exciton diffusion. This anisotropy was determined to be caused by the strength of intermolecular coupling along different crystal axes. <sup>162</sup> As such, the *b*-axis exhibits the strongest coupling and was labeled as the fast axis for exciton diffusion. Since the TAM images were collected in the *ab*-plane, the *a*-axis would then be the slow axis. Further investigation of the tetracene single crystals showed that singlet exciton diffusion exhibited similar anisotropy. A strong coupling between triplet and singlet transport was observed which resulted in a 10x enhancement in the diffusion constant for triplet excitons. Even though SF is comparatively slow in tetracene due to its endothermic nature, the equilibrium between singlet and triplet excitons leads to better and faster long-range transport and can promote its usefulness in optoelectronic devices.

In contrast, using quantum chemical and kinetic random-walk simulations, Xie and Ma observed anisotropy opposite to that observed experimentally for crystalline tetracene. <sup>169</sup> They showed that while exciton diffusion was anisotropic, the preferred directions differed significantly to experimental results: the dominant distribution of singlet diffusion was found to be along the *b*-axis and triplet diffusion was along the *a*-axis. The direction of singlet exciton diffusion was attributed to the greatest exciton coupling in the

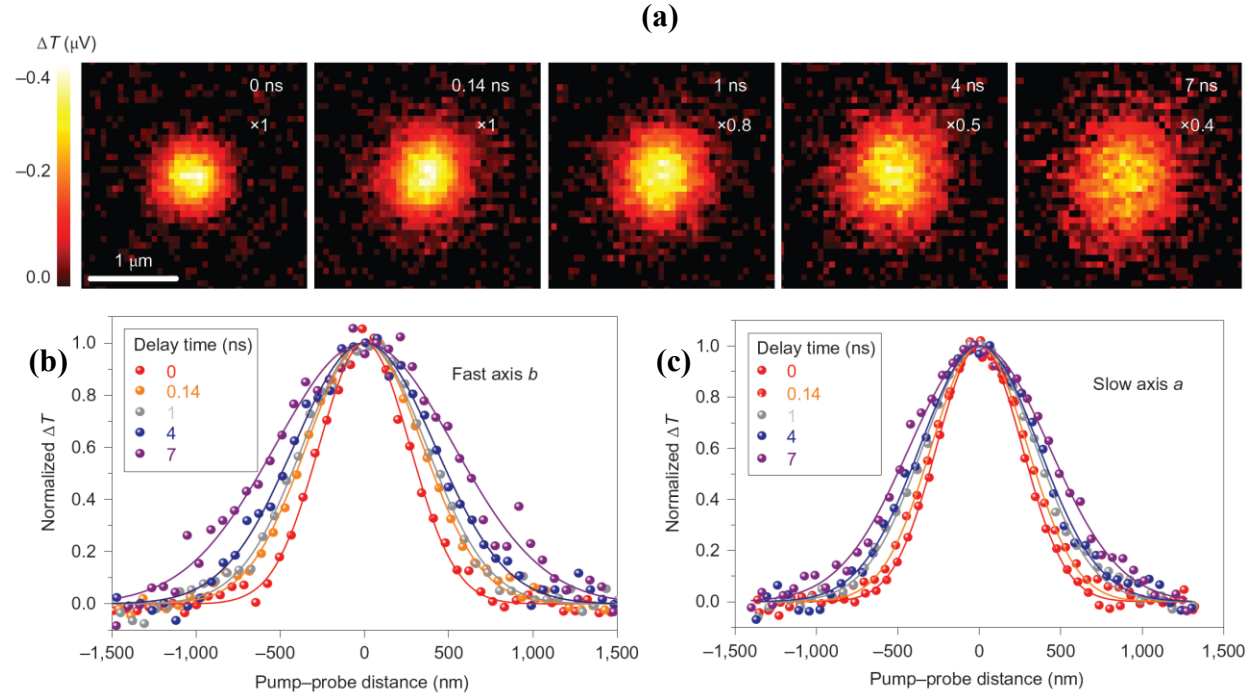


**Figure 16.** Transient absorption microscopy of triplet diffusion in single-crystalline tetracene: (a) triplet diffusion at different time delays, diffusion plots along the (b) *b*- and (c) *a*-axes. (Y. Wan et al., Nature Chem. 7 785(2015).)

same direction. Even though triplet coupling is minimal along the *a*-axis, the major coupling was in the *ab*-direction which resulted in triplet exciton diffusion along the *a*-axis. The reasons for the discrepancy between theoretical and experimental results is unclear and should be studied further.

More recently, Hudson et al. were able to quantify triplet exciton diffusion in TIPS-pentacene using TA spectroscopy, showing that diffusion along the crystal's *a*-axis was over an order of magnitude more prominent than in other directions. <sup>170</sup> By extracting the kinetic data from the TA experiments as shown in Figure 17 and fitting it to a model which assumed isotropic diffusion, anisotropic diffusion was confirmed. By changing the model to consider prominent diffusion along one crystal axis, the process was physically reasonable, and it was determined that triplet diffusion in the functionalized sample on a ps-ns timescale was highly anisotropic. DFT analysis of the system indicated that diffusion along the *a*-axis was 25x faster than other directions. Investigating this adapted acene system highlighted the importance of dictating crystal packing structure when designing and building SF devises with optimal efficiency.

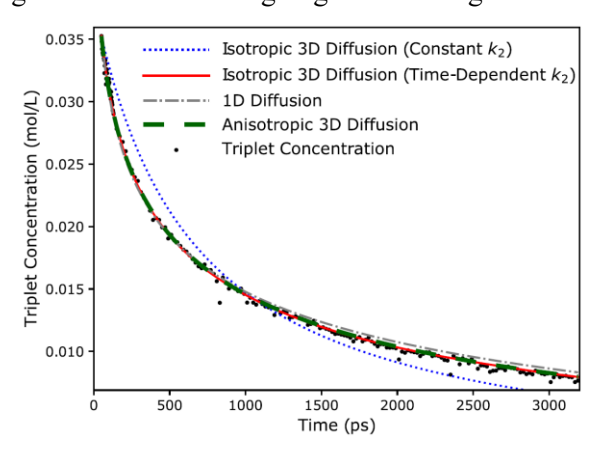


**Figure 17.** Experimental and calculated triplet exciton calculations over time in single-crystalline TIPS-pentacene. Reproduced with permission from J. Phys. Chem. C. **124** (2020) 23541. Copyright 2020 American Chemical Society.

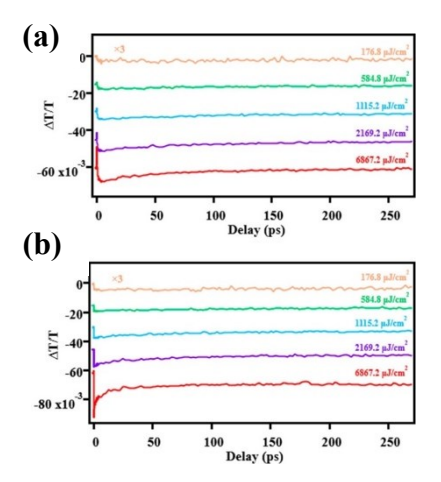


**Figure 18.** Fluence-dependent time traces from transient absorption measurements of single-crystalline hexacene along the (a) *a*- and (b) *b*-axes. Reproduced with permission from J. Phys. Chem. Lett. **11** (2020) 1261. Copyright 2020 American Chemical Society.

Another recent study has used TA microscopy to investigate triplet diffusion in single crystalline hexacene. The dynamical behavior of triplets was studied by monitoring their kinetics under different excitation intensities and faster recovery was observed under high fluence, as shown in Figures 18(a) and (b). Interestingly, no additional features were observed as have been under low fluence. The furthermore, the enhanced recovery rate under high intensity excitation was observed along both a and b crystal axes, although the increased recovery rates were shown to be anisotropic. To this effect, triplet recombination was shown to occur earlier along the b-axis than along the a-axis. This work also compared recombination rates in hexacene polycrystalline thin films to those in single-crystal sample and found that recombination in the thin films occurred at a rate that was the average between the rates along the a- and b-axes of the single crystal sample.

Further analysis of the fluence-dependent triplet kinetics shown in Figure 19 determined that two distinct relaxation processes occur in crystalline samples: one being fluence-dependent and the other being

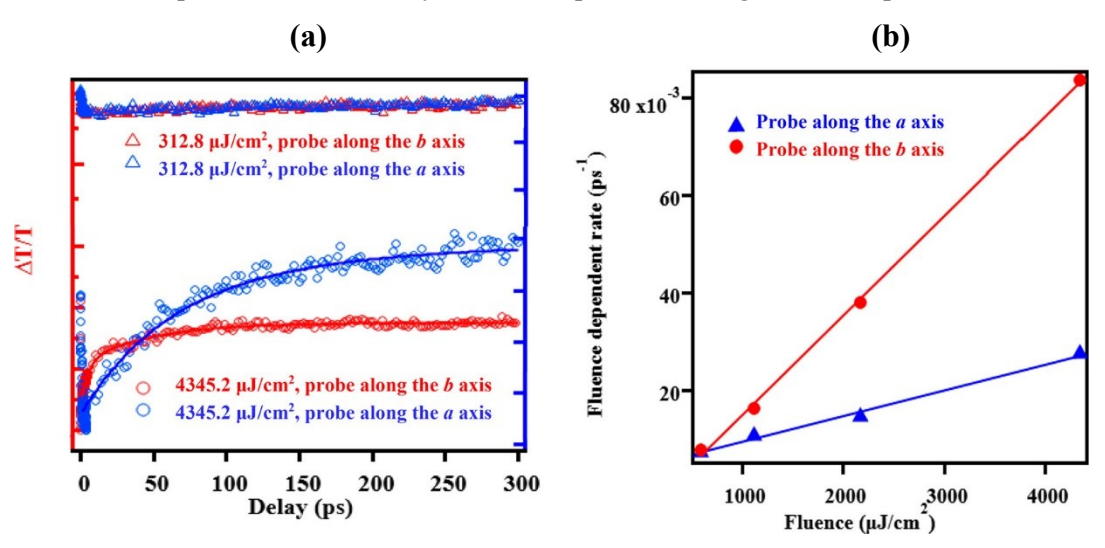


**Figure 19.** (a) Time traces from transient absorption measurements of single-crystalline hexacene at different fluences along the a- (blue) and b-axes (red), (b) anisotropy of fluence dependence of triplet diffusion along the a- and b-axes.

Reproduced with permission from J. Phys. Chem. Lett. 11 (2020) 1261. Copyright 2020 American Chemical Society.

fluence-independent, with the independent process being slower than its fluence-dependent counterpart.

Using a double exponential function do fit the kinetic traces as shown in Figure 19(a), the fast components of recombination along the *a*- and *b*-axes were determined to take 36.3 and 11.9 ps, with slow components of 135.4. and 202.0 ps, respectively. It was also found that the fluence-dependence of the fast component was also anisotropic, as shown in Figure 19(b). The differences in fast and slow rate components for triplet diffusion for the different crystal axes confirms that triplet exciton motion in hexacene single crystals is, in fact, anisotropic.

Han et al. made further considerations to better understand the anisotropic nature of triplet diffusion in hexacene single crystals.<sup>55</sup> They supposed that the trait was a due to a mixture of geminate and nongeminate recombinations or energy transfers. Geminate energy transfer occurs when non-correlated triplet exciton pairs recombine in a monomolecular process. Non-geminate energy transfer occurs when excitons diffuse through a material and recombine bimolecularly later on. The authors suggest that the triplets relax in parallel through both processes, explained by a phenomenological model to provide quantitation.<sup>55</sup> The rate constants for the geminate process were determined to be about 0.0074 and 0.005 ps<sup>-1</sup> along the a and b crystal axes, respectively. Conversely, the rate of the non-geminate process is fluence-dependent and is thereby diffusion-limited through energy transfer. This bimolecular process was found to be almost four times faster along the b-axis than the a-axis. It was also determined that this process is dependent of molecular orientation in the crystalline sample. Recent calculations have shown that the anisotropy in triplet exciton diffusion is the result of anisotropic energy change between the correlated and separate triplet pairs as well as molecular configuration.<sup>53</sup> Referring back to Figure 5(a), the crystal structure for hexacene, molecular orientation along the b-axis is head-to-tail and J-type while it is face-to-face and H-type along the a-axis. H-type configuration results in destructive interference in coupling probability and decreases the rate of exciton recombination relative to J-type ordering. This aligns with the experimental observations of anisotropic diffusion in single crystalline hexacene. Lastly, it was observed that recombination through the non-geminate process was much slower in polycrystalline thin film hexacene, likely caused by sample defects and grain boundaries.

Irkhin and Biaggio employed localized photoexcitation and spatially resolved detection of excitonic luminescence to map out exciton diffusion in rubrene single crystals. The study revealed that exciton mobility in rubrene is significantly anisotropic, with long-distance diffusion spanning several micrometers occurring exclusively along the direction of molecular stacking in the crystal, specifically the b axis. Furthermore, the researchers have determined a triplet diffusion length of 4 micrometers along the b axis of these rubrene single crystals.

# 8. Anisotropic Spin Dynamics in Organic Semiconductors

The correlated triplet pair, ¹(TT), the intermediate formed in the SF processes, possesses characteristics which are both interesting and practically useful. Importantly, the electrons in the ¹(TT) are spin correlated, and their subsequent decoherence underpins the harvesting process of generated excitons which is essential to overall SF efficiency. Accordingly, we will describe some of the recent progresses made in understanding spin dynamics in acenes relevant to singlet fission. The two electrons in the ¹(TT) are delocalized between two adjacent molecules. There are also sublevels which are split from ¹(TT): three triplet ³(TT)'s and five quintet ⁵(TT)'s, whose occupation probabilities rely on the degree of interaction between the adjacent molecules. These substates can tell us more about the physics of the triplet pair and have interesting properties of their ow. For instance, the ⁵(TT) may be useful in quantum information due to its responsiveness to microwave pulses, high degree of entanglement, and optical measurability. Electron spin resonance spectroscopy (EPR) has been used to study the ⁵(TT) in tetracene derivative single crystals. In fact, Weiss et al used this method to detect strongly coupled triplet pairs with long lifetimes in single crystalline and thin film TIPS-tetracene. ¹¹¹ They found through coherent spin manipulation that exchange-coupled quintet complexes existed alongside weakly coupled triplets. The lifespans of the electron pairs

were measured to be on the order of 3  $\mu$ s where their spins were coherent for nearly 1  $\mu$ s at 10 K. This work showed that triplet pair interactions was more powerful than previously expected, which resulted in the long-lived interactive states.

More recently, Rugg et al investigated the spin dynamics of triplet pairs in single-crystalline 2-triethylsilyl-5,11-bis(triisopropylsilyl ethynyl) tetra-ceno[2,3-b]thiophene (TES TIPS-TT), in whose structure all molecules share a common z-axis. <sup>172</sup> In this work, angle-dependent time-resolved EPR (TR-EPR) spectra were used to study the kinetics of  $^5$ (TT). The longest decay time of the  $^5$ (TT), 100 ns, was observed when the molecular x-axis was oriented parallel to the applied magnetic field,  $B_0$  (x-axis|| $B_0$ ), followed by z-axis|| $B_0$ , with much faster decays at intermediate orientations. By comparing these angle-dependent TR-EPR spectra to calculations based on the Hamiltonian and nonadiabatic transition theory, it was concluded that z-axis|| $B_0$  resulted in  $^5$ (TT) being strictly from  $^1$ (TT). It was also concluded that separate  $^5$ (TT) populations are formed in distinct pair that dissociate on the order of nanoseconds, which supports the model for strong and weak coupling in electron pairs.

In 2022, Jacobberger et al. used TR-EPR with angular resolution to investigate 5,12-bis(tricyclohexylsilylethynyl)tetracene (TCHS-tetracene) single crystals. <sup>173</sup> Upon photoexcitation, <sup>5</sup>(TT) is produced through SF and the crystal framework allows for uniform spin alignment and thus specific targeting of spin-sublevel transitions. The <sup>5</sup>(TT) states in TCHS-tetracene display notable spin qubit properties like a coherence time of 3 μs at 10k, a population time of 130 μs at 5 K, and stability under ambient conditions. These works have uncovered mechanisms which result in decoherence such as exciton diffusion, dipole coupling, and nuclear interactions, as well as presenting guidelines for physical conditions like temperature.

More recently, a pentacene/tetracene heterodimer was investigated using coherent EPR nutation spectroscopy where transient spin states where identified. 174 Both coherent and noncoherent methods were used to study different population processes which were spin- and orientation-dependent, specifically, multiple simultaneous quintet formation routes were identified. The pulsed EPR experiments suggest that the formation of quintet multiexcitons influences triplet populations, opposed to the previous attribution of polarization flips to the anisotropic decay of the triplets. This work showed that by tailoring molecular arrangement of SF materials, they could be used for generating multiple electron spins in distinct quantum states.

Table 1. Summary of SF anisotropic SF character in acene semiconductor crystals.

		Tetracen	Pentacene	Hexacene	TIPS-	Method
		e			Pentacene	
Davydov Splitting (eV)	$DS(S_1)$	$0.075_{102}^{102} \\ 0.078_{175}^{175}$	$0.121_{52}^{52} \\ 0.128_{52}^{52}$	$0.144^{176} \\ 0.16^{177} \\ 0.18^{80}$		DFT <sup>102,52,54</sup> TA <sup>175,176,177,178,54</sup> Absorption <sup>52</sup> Reflectance <sup>80</sup>
	$DS(T_1)$	0.04 178	0.03 54	0.03 80		
SF Rate Constants (ps <sup>-1</sup> )	$k_{F,a}$		$3.3 \pm 1.6^{54}$	$5.0 \pm 0.2^{178}$		DFT <sup>54</sup> TA <sup>178,54</sup>
	$k_{F,b}$		$8.1 \pm 1.1$ <sup>54</sup>	$4.5 \pm 0.2^{-178}$		
	$k_{QD,a}$		$6.8 \pm 0.5$ <sup>54</sup>	$3.3 \pm 0.2^{178}$		
	$k_{QD,b}$		$5.7 \pm 1.2^{-54}$	$6.7 \pm 0.2^{178}$		
Diffusion constant (cm <sup>2</sup> s <sup>-1</sup> )	$D_{\mathrm{T},a}$	1.35±0.0 1×10 <sup>-3 60</sup> 0.06 <sup>59</sup>			1.06×10 <sup>-3</sup>	PL <sup>60</sup> TA <sup>59,170</sup>
	$D_{\mathrm{T},b}$	2.28±0.0 7×10 <sup>-3 60</sup> 0.10 <sup>59</sup>			4.14×10 <sup>-5</sup>	
	$D_{\mathrm{T},c}$	0.31±0.0 2×10 <sup>-3 60</sup>			<1×10 <sup>-10</sup>	
	$D_{S,a}$	0.85 59				
	$D_{S,b}$	2.8 59				

## 9. Summary and Outlook

In the pursuit of harnessing solar energy more efficiently, linear polyacenes, such as tetracene, pentacene, hexacene and their derivatives, have emerged as powerful model systems for studying singlet fission (SF). Their high efficiencies are particularly conducive to the exploration of SF mechanisms. This article offers a compelling review of the anisotropic characteristics of vibronic coupling, SF, and triplet transport in single crystalline acenes. These findings reveal how crystal orientation and morphology can be carefully manipulated in organic semiconductors to optimize SF efficiency significantly. Further, the quantified effects of anisotropicity have been summaries in Table 1 for tetracene, pentacene, hexacene, and TIPS-pentacene.

The insights presented here spotlight the potential of anisotropic SF dynamics, not only as a crucial tool for elucidating the complexities of SF mechanisms in molecular crystals but also as a driving force for designing superior photovoltaic and photonic devices. The study of exotic physics governed by oriented transition dipoles in a broad range of molecular crystals could also benefit from this approach.

In this context, we have utilized the Functional Mode Electron Transfer Theory (FMET), a critical tool for understanding electron transfer processes in complex systems, as previously applied to charge transfer processes in acenes. We also discused how advanced spectroscopic techniques have provided more profound insights into SF pathways, contributing to enhanced performance of photovoltaic devices through increased conversion efficiency and chemical stability.

The anisotropic nature of SF in polyacene single crystals is a fascinating result of electronic coupling between molecules and the thermodynamic driving force along different crystal axes. These forces guide the formation and separation of the correlated triplet pair, central to the SF process. Thus, by controlling crystal structure through molecular morphology and crystal orientation, and minimizing energy loss, researchers can optimize the overall efficiency of an SF material.

Advanced instrumentation can reveal the underlying SF mechanisms and suggest ways to achieve improved performance and superior triplet yields. While the SF process could double the number of generated excitons, efficiency is highly dependent on factors such as molecular structure, packing, and orientation within a crystalline material. Understanding how these factors interplay with SF anisotropy could inform the design of optimal photovoltaic materials, potentially achieving unprecedented efficiency levels.

However, there are challenges associated with studying and utilizing the anisotropic nature of SF in single crystal polyacenes. For instance, a comprehensive catalog of structural motifs and energetic conditions promoting SF in various materials would be incredibly beneficial. Machine learning has recently been employed to evaluate the viability of different functionalizations to promote SF in organic systems. <sup>179</sup> New methods based on machine learning and quantum chemistry are being developed and applied to understand and manipulate the anisotropic nature of SF better. These innovative methods promise to accelerate the exploration of more functionalizations of SF materials more quickly than conventional methods would allow.

Further research is needed to understand how molecular alignment and orientation are influenced by different environments and how these relationships can be optimized for maximum performance. Many questions remain unanswered regarding the ideal device architectures for efficient exciton diffusion and transport and for making the most of acene anisotropy.

In conclusion, we believe that the future of SF materials and understanding their fundamental mechanisms will rely on a robust, multifaceted approach that harnesses machine learning, quantum chemistry calculations, 2D spectroscopies, and temporal-, spatial, and frequency-resolved electronic and vibrational techniques. Our primary goal is to stimulate further research into anisotropic SF and exciton transport mechanisms, inspiring the development of innovative techniques to deepen our understanding in the field. By harnessing and manipulating the anisotropic nature of SF and exciton transport, we can guide the design of SF materials for a wide range of optoelectronic applications.

\*Corresponding authors: hchen@tacc.utexas.edu (H.N.N.), gchen@honda-ri.com (G. C.), and yi.rao@usu.edu (Y.R).

#### **ACKNOWLEDGMENTS**

This work is supported by Honda Research Institute USA, Inc. Y.R. is also supported by the National Science Foundation under Grant No. [2045084]. G.H.D acknowledges the start-up fund support from Beijing University of Posts and Telecommunications (BUPT). Computational resources were provided by

the Argonne Leadership Computing Facilities at Argonne National Laboratory under Department of Energy contract DE-AC-06CH11357 and by the Extreme Science and Engineering Discovery Environment at Texas Advanced Computing Center under National Science Foundation contract TG-CHE130008.

# **AUTHOR DECLARATIONS Competing interests**

The authors declare no competing financial interests.

## **REFERENCES:**

- <sup>1</sup> J. Pastuszak, and P. Węgierek, "Photovoltaic Cell Generations and Current Research Directions for Their Development," Materials **15** (2022) 5542.
- <sup>2</sup> M. B. Smith, and J. Michl, "Singlet fission," Chem. Rev. **110** (2010) 6891.
- <sup>3</sup> M. B. Smith, and J. Michl, "Recent advances in singlet fission," Annu. Rev. Phys. Chem. **64** (2013) 361.
- <sup>4</sup>R. Merrifield, P. Avakian, and R. Groff, "Fission of singlet excitons into pairs of triplet excitons in tetracene crystals," Chem. Phys. Lett. **3** (1969) 386.
- <sup>5</sup> G. D. Scholes, "Correlated pair states formed by singlet fission and exciton–exciton annihilation," J. Phys. Chem. C **119** (2015) 12699.
- <sup>6</sup> E. Frankevich, V. Lesin, and A. Pristupa, "Rate constants of singlet exciton fission in a tetracene crystal determined from the rydmr spectral linewidth," Chem. Phys. Lett. **58** (1978) 127.
- <sup>7</sup> J. J. Burdett, and C. J. Bardeen, "Quantum beats in crystalline tetracene delayed fluorescence due to triplet pair coherences produced by direct singlet fission," J. Am. Chem. Soc. **134** (2012) 8597.
- <sup>8</sup> R. D. Pensack, E. E. Ostroumov, A. J. Tilley, S. Mazza, C. Grieco, K. J. Thorley, J. B. Asbury, D. S. Seferos, J. E. Anthony, and G. D. Scholes, "Observation of two triplet-pair intermediates in singlet exciton fission," J. Phys. Chem. Lett. 7 (2016) 2370.
- <sup>9</sup> W.-L. Chan, M. Ligges, A. Jailaubekov, L. Kaake, L. Miaja-Avila, and X.-Y. Zhu, "Observing the multiexciton state in singlet fission and ensuing ultrafast multielectron transfer," Science **334** (2011) 1541.
- <sup>10</sup> A. J. Musser, M. Liebel, C. Schnedermann, T. Wende, T. B. Kehoe, A. Rao, and P. Kukura, "Evidence for conical intersection dynamics mediating ultrafast singlet exciton fission," Nat. Phys. **11** (2015) 352.
- <sup>11</sup> A. A. Bakulin, S. E. Morgan, T. B. Kehoe, M. W. B. Wilson, A. W. Chin, D. Zigmantas, D. Egorova, and A. Rao, "Real-time observation of multiexcitonic states in ultrafast singlet fission using coherent 2D electronic spectroscopy," Nat. Chem. **8** (2016) 16.
- <sup>12</sup> W. Shockley, and H. J. Queisser, "Detailed Balance Limit of Efficiency of p-n Junction Solar Cells," Journal of Applied Physics **32** (1961) 510.
- <sup>13</sup> K. Miyata, F. S. Conrad-Burton, F. L. Geyer, and X. Y. Zhu, "Triplet Pair States in Singlet Fission," Chemical Reviews **119** (2019) 4261.

- <sup>14</sup> T. Ullrich, D. Munz, and D. M. Guldi, "Unconventional singlet fission materials," Chemical Society Reviews **50** (2021) 3485.
- <sup>15</sup> S. Singh, W. Jones, W. Siebrand, B. Stoicheff, and W. Schneider, "Laser generation of excitons and fluorescence in anthracene crystals," J. Chem. Phys. **42** (1965) 330.
- <sup>16</sup> N. Geacintov, M. Pope, and F. Vogel, "Effect of magnetic field on the fluorescence of tetracene crystals: exciton fission," Phys. Rev. Lett. **22** (1969) 593.
- <sup>17</sup> R. E. Merrifield, "Magnetic effects on triplet exciton interactions," Pure Appl. Chem. **27** (1971) 481.
- <sup>18</sup> N. E. Geacintov, M. Binder, C. E. Swenberg, and M. Pope, "Exciton dynamics in α-particle tracks in organic crystals: Magnetic field study of the scintillation in tetracene crystals," Phys. Rev. B **12** (1975) 4113.
- <sup>19</sup> W. G. Albrecht, H. Coufal, R. Haberkorn, and M. E. Michel-Beyerle, "Excitation Spectra of Exciton Fission in Organic Crystals," Phys. Status Solidi B **89** (1978) 261.
- <sup>20</sup> M. C. Hanna, and A. J. Nozik, "Solar conversion efficiency of photovoltaic and photoelectrolysis cells with carrier multiplication absorbers," J. Appl. Phys. **100** (2006) 074510.
- <sup>21</sup> A. J. Baldacchino, M. I. Collins, M. P. Nielsen, T. W. Schmidt, D. R. McCamey, and M. J. Y. Tayebjee, "Singlet fission photovoltaics: Progress and promising pathways," Chem. Phys. Rev. **3** (2022) 021304.
- <sup>22</sup> A. J. Nozik, "Quantization effects in semiconductor nanostructures and singlet fission in molecular chromophores for photovoltaics and solar fuels," Chem. Phys. Rev. **2** (2021) 021305.
- <sup>23</sup> V. Gray, J. R. Allardice, Z. Zhang, and A. Rao, "Organic-quantum dot hybrid interfaces and their role in photon fission/fusion applications," Chem. Phys. Rev. **2** (2021) 031305.
- <sup>24</sup> J. Lee, P. Jadhav, and M. Baldo, "High efficiency organic multilayer photodetectors based on singlet exciton fission," Appl. Phys. Lett. **95** (2009) 192.
- <sup>25</sup> R. Casillas, I. Papadopoulos, T. Ullrich, D. Thiel, A. Kunzmann, and D. M. Guldi, "Molecular insights and concepts to engineer singlet fission energy conversion devices," Energy Environ. Sci. **13** (2020) 2741.
- <sup>26</sup> P. J. Jadhav, A. Mohanty, J. Sussman, J. Lee, and M. A. Baldo, "Singlet Exciton Fission in Nanostructured Organic Solar Cells," Nano Lett. **11** (2011) 1495.
- <sup>27</sup> T. C. Wu, N. J. Thompson, D. N. Congreve, E. Hontz, S. R. Yost, T. Van Voorhis, and M. A. Baldo, "Singlet fission efficiency in tetracene-based organic solar cells," Appl. Phys. Lett. **104** (2014) 193901.
- <sup>28</sup> A. B. Pun, S. N. Sanders, E. Kumarasamy, M. Y. Sfeir, D. N. Congreve, and L. M. Campos, "Triplet Harvesting from Intramolecular Singlet Fission in Polytetracene," Adv. Mater. **29** (2017) 1701416.

- <sup>29</sup> R. W. MacQueen, M. Liebhaber, J. Niederhausen, M. Mews, C. Gersmann, S. Jäckle, K. Jäger, M. J. Y. Tayebjee, T. W. Schmidt, B. Rech, and K. Lips, "Crystalline silicon solar cells with tetracene interlayers: the path to silicon-singlet fission heterojunction devices," Mater. Horiz. **5** (2018) 1065.
- <sup>30</sup> P. D. Reusswig, D. N. Congreve, N. J. Thompson, and M. A. Baldo, "Enhanced external quantum efficiency in an organic photovoltaic cell via singlet fission exciton sensitizer," Appl. Phys. Lett. **101** (2012) 113304.
- <sup>31</sup> A. K. Pandey, "Highly efficient spin-conversion effect leading to energy up-converted electroluminescence in singlet fission photovoltaics," Sci. Rep. **5** (2015) 7787.
- <sup>32</sup> Y. L. Lin, M. A. Fusella, O. V. Kozlov, X. Lin, A. Kahn, M. S. Pshenichnikov, and B. P. Rand, "Morphological Tuning of the Energetics in Singlet Fission Organic Solar Cells," Adv. Funct. Mater. **26** (2016) 6489.
- <sup>33</sup> D. N. Congreve, J. Lee, N. J. Thompson, E. Hontz, S. R. Yost, P. D. Reusswig, M. E. Bahlke, S. Reineke, T. Van Voorhis, and M. A. Baldo, "External Quantum Efficiency Above 100% in a Singlet-Exciton-Fission-Based Organic Photovoltaic Cell," Science **340** (2013) 334.
- <sup>34</sup>B. Ehrler, M. W. B. Wilson, A. Rao, R. H. Friend, and N. C. Greenham, "Singlet Exciton Fission-Sensitized Infrared Quantum Dot Solar Cells," Nano Lett. **12** (2012) 1053.
- <sup>35</sup>B. Ehrler, K. P. Musselman, M. L. Böhm, R. H. Friend, and N. C. Greenham, "Hybrid pentacene/a-silicon solar cells utilizing multiple carrier generation via singlet exciton fission," Appl. Phys. Lett. **101** (2012) 153507
- <sup>36</sup>B. Ehrler, B. J. Walker, M. L. Böhm, M. W. B. Wilson, Y. Vaynzof, R. H. Friend, and N. C. Greenham, "In situ measurement of exciton energy in hybrid singlet-fission solar cells," Nat. Commun. **3** (2012) 1019.
- <sup>37</sup> M. Tabachnyk, B. Ehrler, S. Gélinas, M. L. Böhm, B. J. Walker, K. P. Musselman, N. C. Greenham, R. H. Friend, and A. Rao, "Resonant energy transfer of triplet excitons from pentacene to PbSe nanocrystals," Nat. Mater. **13** (2014) 1033.
- <sup>38</sup> N. J. Thompson, M. W. B. Wilson, D. N. Congreve, P. R. Brown, J. M. Scherer, Thomas S. Bischof, M. Wu, N. Geva, M. Welborn, T. V. Voorhis, V. Bulović, M. G. Bawendi, and Marc A. Baldo, "Energy harvesting of non-emissive triplet excitons in tetracene by emissive PbS nanocrystals," Nat. Mater. **13** (2014) 1039.
- <sup>39</sup> L. Yang, M. Tabachnyk, S. L. Bayliss, M. L. Böhm, K. Broch, N. C. Greenham, R. H. Friend, and B. Ehrler, "Solution-Processable Singlet Fission Photovoltaic Devices," Nano Lett. **15** (2015) 354.
- <sup>40</sup>L. M. Pazos-Outón, J. M. Lee, M. H. Futscher, A. Kirch, M. Tabachnyk, R. H. Friend, and B. Ehrler, "A Silicon–Singlet Fission Tandem Solar Cell Exceeding 100% External Quantum Efficiency with High Spectral Stability," ACS Energy Lett. **2** (2017) 476.

- <sup>41</sup> R. Nagata, H. Nakanotani, W. J. Potscavage Jr., and C. Adachi, "Exploiting Singlet Fission in Organic Light-Emitting Diodes," Adv. Mater. **30** (2018) 1801484.
- <sup>42</sup> J. S. Hub, and B. L. de Groot, "Detection of Functional Modes in Protein Dynamics," PLoS Comput Biol **5** (2009) e1000480.
- <sup>43</sup> H. Chen, "Functional Mode Electron-Transfer Theory," J. Phys. Chem. C **118** (2014) 7586.
- <sup>44</sup> J. E. Elenewski, J. Y. Cai, W. Jiang, and H. Chen, "Functional Mode Hot Electron Transfer Theory," The Journal of Physical Chemistry C **120** (2016) 20579.
- <sup>45</sup> Q. Wu, and T. Van Voorhis, "Direct optimization method to study constrained systems within density-functional theory," Phys. Rev. A **72** (2005) 024502.
- <sup>46</sup> Q. Wu, B. Kaduk, and T. Van Voorhis, "Constrained density functional theory based configuration interaction improves the prediction of reaction barrier heights," J. Chem. Phys. **130** (2009) 034109.
- <sup>47</sup> A. D. Becke, "A multicenter numerical integration scheme for polyatomic molecules," J. Chem. Phys. **88** (1988) 2547.
- <sup>48</sup> M. E. Casida, and M. Huix-Rotllant, "Progress in Time-Dependent Density-Functional Theory," Annu. Rev. Phys. Chem. **63** (2012) 287.
- <sup>49</sup> J. G. Kirkwood, "Statistical Mechanics of Fluid Mixtures," J. Chem. Phys. **3** (1935) 300.
- <sup>50</sup> J. Verbeek, and J. H. Van Lenthe, "On the evaluation of non-orthogonal matrix elements," J. Mol. Struct. **229** (1991) 115.
- <sup>51</sup> A. Farazdel, M. Dupuis, E. Clementi, and A. Aviram, "Electric-field induced intramolecular electron transfer in spiro .pi.-electron systems and their suitability as molecular electronic devices. A theoretical study," J. Am. Chem. Soc. **112** (1990) 4206.
- <sup>52</sup> N. J. Hestand, H. Yamagata, B. Xu, D. Sun, Y. Zhong, A. R. Harutyunyan, G. Chen, H.-L. Dai, Y. Rao, and F. C. Spano, "Polarized Absorption in Crystalline Pentacene: Theory vs Experiment," The Journal of Physical Chemistry C **119** (2015) 22137.
- <sup>53</sup> D. Sun, G.-H. Deng, B. Xu, E. Xu, X. Li, Y. Wu, Y. Qian, Y. Zhong, C. Nuckolls, A. R. Harutyunyan, H.-L. Dai, G. Chen, H. Chen, and Y. Rao, "Anisotropic Singlet Fission in Single Crystalline Hexacene," iScience **19** (2019) 1079.
- <sup>54</sup> G.-H. Deng, Y. Qian, X. Li, T. Zhang, W. Jiang, A. R. Harutyunyan, G. Chen, H. Chen, and Y. Rao, "Singlet Fission Driven by Anisotropic Vibronic Coupling in Single-Crystalline Pentacene," The Journal of Physical Chemistry Letters **12** (2021) 3142.
- <sup>55</sup> J. Han, Q. Xie, J. Luo, G.-H. Deng, Y. Qian, D. Sun, A. R. Harutyunyan, G. Chen, and Y. Rao, "Anisotropic Geminate and Non-Geminate Recombination of Triplet Excitons in Singlet Fission of Single Crystalline Hexacene," J. Phys. Chem. Lett. **11** (2020) 1261.

- <sup>56</sup> Y. Qian, X. Li, A. R. Harutyunyan, G. Chen, Y. Rao, and H. Chen, "Herzberg–Teller Effect on the Vibrationally Resolved Absorption Spectra of Single-Crystalline Pentacene at Finite Temperatures," The Journal of Physical Chemistry A **124** (2020) 9156.
- <sup>57</sup> Y. Qian, T. Zhang, X. Li, Y. Rao, and H. Chen, "Herzberg–Teller Effect in Single-Crystalline Hexacene at Finite Temperatures," The Journal of Physical Chemistry C **126** (2022) 3366.
- <sup>58</sup> T. Zhu, Y. Wan, and L. Huang, "Direct Imaging of Frenkel Exciton Transport by Ultrafast Microscopy," Acc. Chem. Res. **50** (2017) 1725.
- <sup>59</sup> Y. Wan, Z. Guo, T. Zhu, S. Yan, J. Johnson, and L. Huang, "Cooperative singlet and triplet exciton transport in tetracene crystals visualized by ultrafast microscopy," Nature Chemistry **7** (2015) 785.
- <sup>60</sup> G. M. Akselrod, P. B. Deotare, N. J. Thompson, J. Lee, W. A. Tisdale, M. A. Baldo, V. M. Menon, and V. Bulović, "Visualization of exciton transport in ordered and disordered molecular solids," Nature Communications **5** (2014) 3646.
- <sup>61</sup>C. Y. Wong, B. L. Cotts, H. Wu, and N. S. Ginsberg, "Exciton dynamics reveal aggregates with intermolecular order at hidden interfaces in solution-cast organic semiconducting films," Nat. Commun. **6** (2015) 5946.
- <sup>62</sup> G. Grancini, D. Polli, D. Fazzi, J. Cabanillas-Gonzalez, G. Cerullo, and G. Lanzani, "Transient Absorption Imaging of P3HT:PCBM Photovoltaic Blend: Evidence For Interfacial Charge Transfer State," J. Phys. Chem. Lett. **2** (2011) 1099.
- <sup>63</sup> W. R. Silva, C. T. Graefe, and R. R. Frontiera, "Toward Label-Free Super-Resolution Microscopy," ACS Photonics **3** (2016) 79.
- <sup>64</sup> A. A. Cassabaum, K. Bera, C. C. Rich, B. R. Nebgen, S. Y. Kwang, M. L. Clapham, and R. R. Frontiera, "Femtosecond stimulated Raman spectro-microscopy for probing chemical reaction dynamics in solid-state materials," J. Chem. Phys. **153** (2020) 030901.
- <sup>65</sup> S. M. Hart, W. R. Silva, and R. R. Frontiera, "Femtosecond stimulated Raman evidence for charge-transfer character in pentacene singlet fission," Chem. Sci. **9** (2018) 1242.
- <sup>66</sup> J. E. Anthony, "Functionalized Acenes and Heteroacenes for Organic Electronics," Chem. Rev. **106** (2006) 5028.
- <sup>67</sup>M. Bendikov, F. Wudl, and D. F. Perepichka, "Tetrathiafulvalenes, Oligoacenenes, and Their Buckminsterfullerene Derivatives: The Brick and Mortar of Organic Electronics," Chem. Rev. **104** (2004) 4891.
- <sup>68</sup> J. E. Anthony, "The Larger Acenes: Versatile Organic Semiconductors," Angew. Chem. Int. Ed. **47** (2008) 452.
- <sup>69</sup> Z. Birech, M. Schwoerer, T. Schmeiler, J. Pflaum, and H. Schwoerer, "Ultrafast dynamics of excitons in tetracene single crystals," J. Chem. Phys. **140** (2014) 114501.

- <sup>70</sup> C. Tönshoff, and H. F. Bettinger, "Pushing the Limits of Acene Chemistry: The Recent Surge of Large Acenes," Chem. Eur. J **27** (2021) 3193.
- <sup>71</sup>R. Mondal, C. Tönshoff, D. Khon, D. C. Neckers, and H. F. Bettinger, "Synthesis, Stability, and Photochemistry of Pentacene, Hexacene, and Heptacene: A Matrix Isolation Study," J. Am. Chem. Soc. **131** (2009) 14281.
- <sup>72</sup> Y. Tomkiewicz, R. Groff, and P. Avakian, "Spectroscopic approach to energetics of exciton fission and fusion in tetracene crystals," J. Chem. Phys. **54** (1971) 4504.
- <sup>73</sup> N. Geacintov, J. Burgos, M. Pope, and C. Strom, "Heterofission of pentacene excited singlets in pentacene-doped tetracene crystals," Chem. Phys. Lett. **11** (1971) 504.
- <sup>74</sup> M. Einzinger, T. Wu, J. F. Kompalla, H. L. Smith, C. F. Perkinson, L. Nienhaus, S. Wieghold, D. N. Congreve, A. Kahn, M. G. Bawendi, and M. A. Baldo, "Sensitization of silicon by singlet exciton fission in tetracene," Nature **571** (2019) 90.
- <sup>75</sup> M. W. Wilson, A. Rao, B. Ehrler, and R. H. Friend, "Singlet exciton fission in polycrystalline pentacene: from photophysics toward devices," Acc. Chem. Res. **46** (2013) 1330.
- <sup>76</sup> A. D. M. a. A. Wilkinson, *IUPAC*. Compendium of Chemical Terminology, 2nd ed. (the "Gold Book") (Blackwell Scientific Publications, Oxford, 1997), 2nd edn.,
- <sup>77</sup> A. S. Davydov, "The theory of molecular excitons," Soviet Physics Uspekhi 7 (1964) 145.
- <sup>78</sup> A. Davydov, "Theory of absorption spectra of molecular crystals," Transl. Repr. from Zh. Eksp. Teor. Fiz. **18** (1948) 210.
- <sup>79</sup> H. Ohigashi, I. Shirotani, H. Inokuchi, and S. Minomura, "Effect of Pressure on Davydov Splitting of Tetracene Crystals," J. Chem. Phys. **43** (1965) 314.
- <sup>80</sup> A. Chernikov, O. Yaffe, B. Kumar, Y. Zhong, C. Nuckolls, and T. F. Heinz, "Spectroscopic Study of Anisotropic Excitons in Single Crystal Hexacene," The Journal of Physical Chemistry Letters **5** (2014) 3632.
- <sup>81</sup> A. Bree, and L. E. Lyons, "1002. The intensity of ultraviolet-light absorption by monocrystals. Part IV. Absorption by naphthacene of plane-polarized light," J. Chem. Soc. (1960) 5206.
- <sup>82</sup> B. A. West, J. M. Womick, L. E. McNeil, K. J. Tan, and A. M. Moran, "Ultrafast Dynamics of Frenkel Excitons in Tetracene and Rubrene Single Crystals," J. Phys. Chem. C **114** (2010) 10580.
- <sup>83</sup> V. Zanker, and J. Preuss, "Microspectrometrical Measurements on Single Crystals of Tetracene and Pentacene in Depedence of Thickness and Temperature," Z. Angew. Phys. **27** (1969) 363.
- <sup>84</sup> E. Busby, T. C. Berkelbach, B. Kumar, A. Chernikov, Y. Zhong, H. Hlaing, X.-Y. Zhu, T. F. Heinz, M. S. Hybertsen, and M. Y. Sfeir, "Multiphonon relaxation slows singlet fission in crystalline hexacene," J. Am. Chem. Soc. **136** (2014) 10654.

- <sup>85</sup> D. W. Schlosser, and M. R. Philpott, "Singlet excitons in crystalline naphthalene, antracene, tetracene and pentacene," Chem. Phys. **49** (1980) 181.
- <sup>86</sup> R. Schuster, M. Knupfer, and H. Berger, "Exciton Band Structure of Pentacene Molecular Solids: Breakdown of the Frenkel Exciton Model," Phys. Rev. Lett. **98** (2007) 037402.
- <sup>87</sup>L. Sebastian, G. Weiser, and H. Bässler, "Charge transfer transitions in solid tetracene and pentacene studied by electroabsorption," Chem. Phys. **61** (1981) 125.
- <sup>88</sup> L. Sebastian, G. Weiser, G. Peter, and H. Bässler, "Charge-transfer transitions in crystalline anthracene and their role in photoconductivity," Chem. Phys. **75** (1983) 103.
- <sup>89</sup> Q. Yang, M. Muntwiler, and X. Y. Zhu, "Charge transfer excitons and image potential states on organic semiconductor surfaces," Phys. Rev. B **80** (2009) 115214.
- <sup>90</sup> X. Y. Zhu, Q. Yang, and M. Muntwiler, "Charge-Transfer Excitons at Organic Semiconductor Surfaces and Interfaces," Acc. Chem. Res. **42** (2009) 1779.
- <sup>91</sup> B. Petelenz, P. Petelenz, H. F. Shurvell, and V. H. Smith, "Reconsideration of the electroabsorption spectra of the tetracene and pentacene crystals," Chem. Phys. **119** (1988) 25.
- <sup>92</sup> M. L. Tiago, J. E. Northrup, and S. G. Louie, "Ab initio calculation of the electronic and optical properties of solid pentacene," Phys. Rev. B **67** (2003) 115212.
- 93 H. Yamagata, J. Norton, E. Hontz, Y. Olivier, D. Beljonne, J. L. Brédas, R. J. Silbey, and F. C. Spano,
- "The nature of singlet excitons in oligoacene molecular crystals," J. Chem. Phys. 134 (2011) 204703.
- <sup>94</sup> M. R. Philpott, "Dipole Davydov Splittings in Crystalline Anthracene, Tetracene, Naphthalene, and Phenanthrene," J. Chem. Phys. **50** (1969) 5117.
- <sup>95</sup> A. Prikhotko, and L. Tsikora, "Spectral Investigations of Pentacene," Opt. Spectrosc. **25** (1968) 242.
- <sup>96</sup> T. Aoki-Matsumoto, K. Furuta, T. Yamada, H. Moriya, K. Mizuno, and A. H. Matsui, "Excitonic Photoluminescene in Pentacene Single Crystal," Int. J. Mod. Phys. B **15** (2001) 3753.
- <sup>97</sup> Y. Qian, T. Zhang, J. Han, A. R. Harutyunyan, G. Chen, Y. Rao, and H. Chen, "Symmetry-Breaking Enhanced Herzberg–Teller Effect with Brominated Polyacenes," J. Phys. Chem. C **125** (2021) 3589.
- <sup>98</sup> G.-H. Deng, Q. Wei, J. Han, Y. Qian, J. Luo, A. R. Harutyunyan, G. Chen, H. Bian, H. Chen, and Y. Rao, "Vibronic fingerprint of singlet fission in hexacene," J. Chem. Phys. **151** (2019) 054703.
- <sup>99</sup> W. Kim, and A. J. Musser, "Tracking ultrafast reactions in organic materials through vibrational coherence: vibronic coupling mechanisms in singlet fission," Adv. Phys.: X **6** (2021) 1918022.
- <sup>100</sup> H. Kim, and P. M. Zimmerman, "Coupled double triplet state in singlet fission," Phys. Chem. Chem. Phys. **20** (2018) 30083.
- <sup>101</sup> A. Manian, and S. P. Russo, "The dominant nature of Herzberg–Teller terms in the photophysical description of naphthalene compared to anthracene and tetracene," Sci. Rep. **12** (2022) 21481.

- <sup>102</sup> H. Yamagata, J. Norton, E. Hontz, Y. Olivier, D. Beljonne, J. L. Brédas, R. J. Silbey, and F. C. Spano, "The nature of singlet excitons in oligoacene molecular crystals," The Journal of Chemical Physics **134** (2011)
- <sup>103</sup> D. Beljonne, H. Yamagata, J. L. Brédas, F. C. Spano, and Y. Olivier, "Charge-Transfer Excitations Steer the Davydov Splitting and Mediate Singlet Exciton Fission in Pentacene," Physical Review Letters **110** (2013) 226402.
- <sup>104</sup> S. Sharifzadeh, P. Darancet, L. Kronik, and J. B. Neaton, "Low-Energy Charge-Transfer Excitons in Organic Solids from First-Principles: The Case of Pentacene," The Journal of Physical Chemistry Letters **4** (2013) 2197.
- <sup>105</sup> E. C. Greyson, J. Vura-Weis, J. Michl, and M. A. Ratner, "Maximizing Singlet Fission in Organic Dimers: Theoretical Investigation of Triplet Yield in the Regime of Localized Excitation and Fast Coherent Electron Transfer," The Journal of Physical Chemistry B **114** (2010) 14168.
- <sup>106</sup> W.-L. Chan, M. Ligges, and X. Y. Zhu, "The energy barrier in singlet fission can be overcome through coherent coupling and entropic gain," Nature Chemistry **4** (2012) 840.
- <sup>107</sup> N. R. Monahan, D. Sun, H. Tamura, K. W. Williams, B. Xu, Y. Zhong, B. Kumar, C. Nuckolls, A. R. Harutyunyan, G. Chen, H.-L. Dai, D. Beljonne, Y. Rao, and X. Y. Zhu, "Dynamics of the triplet-pair state reveals the likely coexistence of coherent and incoherent singlet fission in crystalline hexacene," Nature Chemistry **9** (2017) 341.
- <sup>108</sup> C. Y. Wong, S. B. Penwell, B. L. Cotts, R. Noriega, H. Wu, and N. S. Ginsberg, "Revealing exciton dynamics in a small-molecule organic semiconducting film with subdomain transient absorption microscopy," J. Phys. Chem. C **117** (2013) 22111.
- <sup>109</sup> B. Zhang, C. Zhang, Y. Xu, R. Wang, B. He, Y. Liu, S. Zhang, X. Wang, and M. Xiao, "Polarization-dependent exciton dynamics in tetracene single crystals," J. Chem. Phys. **141** (2014) 244303.
- <sup>110</sup> V. K. Thorsmølle, R. D. Averitt, J. Demsar, D. L. Smith, S. Tretiak, R. L. Martin, X. Chi, B. K. Crone, A. P. Ramirez, and A. J. Taylor, "Morphology Effectively Controls Singlet-Triplet Exciton Relaxation and Charge Transport in Organic Semiconductors," Phys. Rev. Lett. **102** (2009) 017401.
- <sup>111</sup> M. W. B. Wilson, A. Rao, K. Johnson, S. Gélinas, R. di Pietro, J. Clark, and R. H. Friend,
- "Temperature-Independent Singlet Exciton Fission in Tetracene," J. Am. Chem. Soc. 135 (2013) 16680.
- <sup>112</sup> J. J. Burdett, A. M. Müller, D. Gosztola, and C. J. Bardeen, "Excited state dynamics in solid and monomeric tetracene: The roles of superradiance and exciton fission," J. Chem. Phys. **133** (2010) 144506.
- <sup>113</sup> Z. Birech, M. Schwoerer, J. Pflaum, and H. Schwoerer, in *Frontiers in Optics* (Optica Publishing Group, 2014), p. FTu1G. 8.

- <sup>114</sup>G. Wang, C. Zhang, Z. Liu, R. Wang, H. Ma, X. Wang, and M. Xiao, "Singlet Fission Dynamics in Tetracene Single Crystals Probed by Polarization-Dependent Two-Dimensional Electronic Spectroscopy," J. Phys. Chem. C **124** (2020) 10447.
- <sup>115</sup> G. B. Piland, and C. J. Bardeen, "How Morphology Affects Singlet Fission in Crystalline Tetracene," J. Phys. Chem. Lett. **6** (2015) 1841.
- <sup>116</sup> D. H. Arias, J. L. Ryerson, J. D. Cook, N. H. Damrauer, and J. C. Johnson, "Polymorphism influences singlet fission rates in tetracene thin films," Chem. Sci. 7 (2016) 1185.
- <sup>117</sup>C. Jundt, G. Klein, B. Sipp, J. Le Moigne, M. Joucla, and A. Villaeys, "Exciton dynamics in pentacene thin films studied by pump-probe spectroscopy," Chem. Phys. Lett. **241** (1995) 84.
- <sup>118</sup> M. W. Wilson, A. Rao, J. Clark, R. S. S. Kumar, D. Brida, G. Cerullo, and R. H. Friend, "Ultrafast dynamics of exciton fission in polycrystalline pentacene," J. Am. Chem. Soc. **133** (2011) 11830.
- <sup>119</sup> A. D. Poletayev, J. Clark, M. W. B. Wilson, A. Rao, Y. Makino, S. Hotta, and R. H. Friend, "Triplet Dynamics in Pentacene Crystals: Applications to Fission-Sensitized Photovoltaics," Adv. Mater. **26** (2014) 919.
- <sup>120</sup> P. M. Zimmerman, Z. Zhang, and C. B. Musgrave, "Singlet fission in pentacene through multi-exciton quantum states," Nat. Chem. **2** (2010) 648.
- <sup>121</sup> P. M. Zimmerman, F. Bell, D. Casanova, and M. Head-Gordon, "Mechanism for singlet fission in pentacene and tetracene: From single exciton to two triplets," J. Am. Chem. Soc. **133** (2011) 19944.
- <sup>122</sup> K. Broch, J. Dieterle, F. Branchi, N. Hestand, Y. Olivier, H. Tamura, C. Cruz, V. Nichols, A. Hinderhofer, and D. Beljonne, "Robust singlet fission in pentacene thin films with tuned charge transfer interactions," Nat. Commun. **9** (2018) 954.
- <sup>123</sup> K. Kolata, T. Breuer, G. Witte, and S. Chatterjee, "Molecular Packing Determines Singlet Exciton Fission in Organic Semiconductors," ACS Nano **8** (2014) 7377.
- $^{124}$ B. D. Folie, J. B. Haber, S. Refaely-Abramson, J. B. Neaton, and N. S. Ginsberg, "Long-Lived Correlated Triplet Pairs in a  $\pi$ -Stacked Crystalline Pentacene Derivative," J. Am. Chem. Soc. **140** (2018) 2326.
- <sup>125</sup> A. C. Jones, N. M. Kearns, J.-J. Ho, J. T. Flach, and M. T. Zanni, "Impact of non-equilibrium molecular packings on singlet fission in microcrystals observed using 2D white-light microscopy," Nat. Chem. **12** (2020) 40.
- <sup>126</sup> F. Anger, J. Ossó, U. Heinemeyer, K. Broch, R. Scholz, A. Gerlach, and F. Schreiber,
- "Photoluminescence spectroscopy of pure pentacene, perfluoropentacene, and mixed thin films," J. Chem. Phys. **136** (2012) 054701.
- <sup>127</sup> A. J. Nozik, "Nanoscience and nanostructures for photovoltaics and solar fuels," Nano Lett. **10** (2010) 2735.

- <sup>128</sup> W.-L. Chan, M. Ligges, and X. Zhu, "The energy barrier in singlet fission can be overcome through coherent coupling and entropic gain," Nat. Chem. **4** (2012) 840.
- <sup>129</sup> H. Seiler, M. Krynski, D. Zahn, S. Hammer, Y. W. Windsor, T. Vasileiadis, J. Pflaum, R. Ernstorfer, M. Rossi, and H. Schwoerer, "Nuclear dynamics of singlet exciton fission in pentacene single crystals," Sci. Adv. 7 (2021) eabg0869.
- <sup>130</sup> A. Ashoka, N. Gauriot, A. V. Girija, N. Sawhney, A. J. Sneyd, K. Watanabe, T. Taniguchi, J. Sung, C. Schnedermann, and A. Rao, "Direct observation of ultrafast singlet exciton fission in three dimensions," Nat. Commun. **13** (2022) 5963.
- <sup>131</sup> J. J. Burdett, D. Gosztola, and C. J. Bardeen, "The dependence of singlet exciton relaxation on excitation density and temperature in polycrystalline tetracene thin films: Kinetic evidence for a dark intermediate state and implications for singlet fission," J. Chem. Phys. **135** (2011) 214508.
- <sup>132</sup> J. E. Elenewski, U. S. Cubeta, E. Ko, and H. Chen, "Functional Mode Singlet Fission Theory," J. Phys. Chem. C **121** (2017) 4130.
- <sup>133</sup> J. E. Elenewski, U. S. Cubeta, E. Ko, and H. Chen, "Computer Simulation of Singlet Fission in Single Crystalline Pentacene by Functional Mode Vibronic Theory," J. Phys. Chem. C **121** (2017) 11159.
- <sup>134</sup> M. Cai, Y. Chen, J. Shinar, O. Mitrofanov, C. Kloc, and A. Ramirez, "Photoluminescence-detected magnetic resonance (PLDMR) study of rubrene and oxygen-doped rubrene films and powders," Proc. SPIE **7415** (2009) 74151Y.
- <sup>135</sup> A. Ryasnyanskiy, and I. Biaggio, "Triplet exciton dynamics in rubrene single crystals," Phys. Rev. B **84** (2011) 193203.
- <sup>136</sup> L. Ma, K. Zhang, C. Kloc, H. Sun, C. Soci, M. E. Michel-Beyerle, and G. G. Gurzadyan, "Fluorescence from rubrene single crystals: Interplay of singlet fission and energy trapping," Phys. Rev. B 87 (2013) 201203.
- <sup>137</sup> L. Ma, K. Zhang, C. Kloc, H. Sun, M. E. Michel-Beyerle, and G. G. Gurzadyan, "Singlet fission in rubrene single crystal: direct observation by femtosecond pump–probe spectroscopy," Phys. Chem. Chem. Phys. **14** (2012) 8307.
- <sup>138</sup> Y. Ishibashi, Y. Inoue, and T. Asahi, "The excitation intensity dependence of singlet fission dynamics of a rubrene microcrystal studied by femtosecond transient microspectroscopy," Photochem. Photobiol. Sci. **15** (2016) 1304.
- <sup>139</sup> K. Miyata, Y. Kurashige, K. Watanabe, T. Sugimoto, S. Takahashi, S. Tanaka, J. Takeya, T. Yanai, and Y. Matsumoto, "Coherent singlet fission activated by symmetry breaking," Nat. Chem. 9 (2017) 983.
  <sup>140</sup> I. Breen, R. Tempelaar, L. A. Bizimana, B. Kloss, D. R. Reichman, and D. B. Turner, "Triplet Separation Drives Singlet Fission after Femtosecond Correlated Triplet Pair Production in Rubrene," J. Am. Chem. Soc. 139 (2017) 11745.

- <sup>141</sup> Y. Liu, X. Yang, L. Ye, H. Ma, and H. Zhu, "Molecular stacking controlling coherent and incoherent singlet fission in polymorph rubrene single crystals," Aggregate (2023) e347.
- <sup>142</sup> J. D. B. Van Schenck, G. Mayonado, J. E. Anthony, M. W. Graham, and O. Ostroverkhova, "Molecular packing-dependent exciton dynamics in functionalized anthradithiophene derivatives: From solutions to crystals," J. Chem. Phys. **153** (2020) 164715.
- <sup>143</sup> Q. Sun, T. Jiang, Q. Ou, Q. Peng, and Z. Shuai, "Influence of Intermolecular Packing on Light Emitting Efficiency and Carrier-Mobility of Organic Semiconductors: Theoretical Descriptor for Molecular Design," Adv. Opt. Mater. **11** (2023) 2202621.
- <sup>144</sup> M. K. Sørensen, A. S. Gertsen, R. P. Fornari, B. Zhou, X. Zhang, P. U. Jepsen, E. Stanzani, S. Yun, M. Fernández Castro, M. Schwartzkopf, A. Koutsioubas, P. de Silva, M. Espindola-Rodriguez, L. T. Kuhn, and J. W. Andreasen, "Manipulating Organic Semiconductor Morphology with Visible Light," Adv. Funct. Mater. **33** (2023) 2212835.
- <sup>145</sup> A. Mohajeri, and M. Farmani, "Toward More Efficient Organic Semiconductors: The Relationship between Morphology, Charge Transport, and Photophysical Properties," ACS Appl. Electron. Mater. **4** (2022) 246.
- <sup>146</sup> Y. Han, W. Ning, L. Cao, X. Xu, T. Li, F. Zhang, L. Pi, F. Xu, and M. Tian, "Photophysical and electrical properties of organic waveguide nanorods of perylene-3,4,9,10-tetracarboxylic dianhydride," Nano Res. **9** (2016) 1948.
- <sup>147</sup> G. Mayonado, K. T. Vogt, J. D. B. Van Schenck, L. Zhu, G. Fregoso, J. Anthony, O. Ostroverkhova, and M. W. Graham, "High-Symmetry Anthradithiophene Molecular Packing Motifs Promote Thermally Activated Singlet Fission," J. Phys. Chem. C **126** (2022) 4433.
- <sup>148</sup> A. K. Le, J. A. Bender, and S. T. Roberts, "Slow singlet fission observed in a polycrystalline perylenediimide thin film," J. Phys. Chem. Lett. **7** (2016) 4922.
- <sup>149</sup> A. K. Le, J. A. Bender, D. H. Arias, D. E. Cotton, J. C. Johnson, and S. T. Roberts, "Singlet fission involves an interplay between energetic driving force and electronic coupling in perylenediimide films," J. Am. Chem. Soc. **140** (2018) 814.
- <sup>150</sup> C. Ramanan, A. L. Smeigh, J. E. Anthony, T. J. Marks, and M. R. Wasielewski, "Competition between Singlet Fission and Charge Separation in Solution-Processed Blend Films of 6,13-Bis(triisopropylsilylethynyl)pentacene with Sterically-Encumbered Perylene-3,4:9,10-bis(dicarboximide)s," J. Am. Chem. Soc. **134** (2012) 386.
- <sup>151</sup> J. Zhou, H. Liu, W. Wang, T. Li, Z. Li, Z. Liu, Y. Chen, Y. Dong, and X. Li, "Influence of core-twisted structure on singlet fission in perylenediimide film," J. Photochem. Photobiol., A **438** (2023) 114473.

- <sup>152</sup> M. L. Williams, I. Schlesinger, C. E. Ramirez, R. M. Jacobberger, P. J. Brown, R. M. Young, and M. R. Wasielewski, "Effect of Crystallinity on Endoergic Singlet Fission in Perylenediimide Single Crystals and Polycrystalline Films," J. Phys. Chem. C **126** (2022) 10287.
- <sup>153</sup> G. D. Scholes, G. R. Fleming, A. Olaya-Castro, and R. Van Grondelle, "Lessons from nature about solar light harvesting," Nat. Chem. **3** (2011) 763.
- <sup>154</sup> M. Escalante, A. Lenferink, Y. Zhao, N. Tas, J. Huskens, C. N. Hunter, V. Subramaniam, and C. Otto, "Long-range energy propagation in nanometer arrays of light harvesting antenna complexes," Nano Lett. **10** (2010) 1450.
- <sup>155</sup> R. R. Lunt, N. C. Giebink, A. A. Belak, J. B. Benziger, and S. R. Forrest, "Exciton diffusion lengths of organic semiconductor thin films measured by spectrally resolved photoluminescence quenching," J. Appl. Phys. **105** (2009) 053711.
- <sup>156</sup> S. M. Menke, W. A. Luhman, and R. J. Holmes, "Tailored exciton diffusion in organic photovoltaic cells for enhanced power conversion efficiency," Nat. Mater. **12** (2013) 152.
- <sup>157</sup> H. Najafov, B. Lee, Q. Zhou, L. C. Feldman, and V. Podzorov, "Observation of long-range exciton diffusion in highly ordered organic semiconductors," Nat. Mater. **9** (2010) 938.
- <sup>158</sup> R. R. Lunt, J. B. Benziger, and S. R. Forrest, "Relationship between Crystalline Order and Exciton Diffusion Length in Molecular Organic Semiconductors," Adv. Mater. **22** (2010) 1233.
- <sup>159</sup> V. Ern, "Anisotropy of Triplet Exciton Diffusion in Anthracene," Phys. Rev. Lett. 22 (1969) 343.
- <sup>160</sup> B. Mulder, "Anisotropy of light absorption and exciton diffusion in anthracene crystals determined from externally sensitized fluorescence," Philips Res. Rep **22** (1967) 142.
- <sup>161</sup> Z. G. Soos, and R. C. Powell, "Generalized Random-Walk Model for Singlet-Exciton Energy Transfer," Phys. Rev. B **6** (1972) 4035.
- <sup>162</sup> S. R. Yost, E. Hontz, S. Yeganeh, and T. Van Voorhis, "Triplet vs Singlet Energy Transfer in Organic Semiconductors: The Tortoise and the Hare," J. Phys. Chem. C **116** (2012) 17369.
- <sup>163</sup> J. R. Lakowicz, *Principles of FLuorescence Spectroscopy* (Springer, 2006), 3rd edn., 507-527.
- <sup>164</sup> S. Speiser, S. Hassoon, and M. B. Rubin, "The mechanism of short-range intramolecular electronic energy transfer in bichromophoric molecules. 2. Triplet-triplet transfer," J. Phys. Chem. **90** (1986) 5085.
- <sup>165</sup> D. L. Dexter, "A theory of sensitized luminescence in solids," J. Chem. Phys. **21** (1953) 836.
- <sup>166</sup> P. Irkhin, and I. Biaggio, "Direct Imaging of Anisotropic Exciton Diffusion and Triplet Diffusion Length in Rubrene Single Crystals," Phys. Rev. Lett. **107** (2011) 017402.
- <sup>167</sup> S. Tavazzi, L. Raimondo, L. Silvestri, P. Spearman, A. Camposeo, M. Polo, and D. Pisignano, "Dielectric tensor of tetracene single crystals: The effect of anisotropy on polarized absorption and emission spectra," J. Chem. Phys. **128** (2008) 154709.

- <sup>168</sup> T. Zhu, Y. Wan, Z. Guo, J. Johnson, and L. Huang, "Two Birds with One Stone: Tailoring Singlet Fission for Both Triplet Yield and Exciton Diffusion Length," Adv. Mater. **28** (2016) 7539.
- <sup>169</sup> X. Xie, and H. Ma, "Opposite anisotropy effects of singlet and triplet exciton diffusion in tetracene crystal," ChemistryOpen **5** (2016) 201.
- <sup>170</sup> R. J. Hudson, D. M. Huang, and T. W. Kee, "Anisotropic Triplet Exciton Diffusion in Crystalline Functionalized Pentacene," The Journal of Physical Chemistry C **124** (2020) 23541.
- <sup>171</sup> L. R. Weiss, S. L. Bayliss, F. Kraffert, K. J. Thorley, J. E. Anthony, R. Bittl, R. H. Friend, A. Rao, N. C. Greenham, and J. Behrends, "Strongly exchange-coupled triplet pairs in an organic semiconductor," Nature Physics **13** (2017) 176.
- <sup>172</sup> B. K. Rugg, K. E. Smyser, B. Fluegel, C. H. Chang, K. J. Thorley, S. Parkin, J. E. Anthony, J. D. Eaves, and J. C. Johnson, "Triplet-pair spin signatures from macroscopically aligned heteroacenes in an oriented single crystal," Proceedings of the National Academy of Sciences **119** (2022) e2201879119.
- <sup>173</sup> R. M. Jacobberger, Y. Qiu, M. L. Williams, M. D. Krzyaniak, and M. R. Wasielewski, "Using Molecular Design to Enhance the Coherence Time of Quintet Multiexcitons Generated by Singlet Fission in Single Crystals," Journal of the American Chemical Society **144** (2022) 2276.
- <sup>174</sup> T. S. C. MacDonald, M. J. Y. Tayebjee, M. I. Collins, E. Kumarasamy, S. N. Sanders, M. Y. Sfeir, L. M. Campos, and D. R. McCamey, "Anisotropic Multiexciton Quintet and Triplet Dynamics in Singlet Fission via Pulsed Electron Spin Resonance," Journal of the American Chemical Society 145 (2023) 15275.
- <sup>175</sup> Z. Birech, M. Schwoerer, T. Schmeiler, J. Pflaum, and H. Schwoerer, "Ultrafast dynamics of excitons in tetracene single crystals," The Journal of Chemical Physics **140** (2014)
- <sup>176</sup> D. Sun, G.-H. Deng, B. Xu, E. Xu, X. Li, Y. Wu, Y. Qian, Y. Zhong, C. Nuckolls, and A. R. Harutyunyan, "Anisotropic singlet fission in single crystalline hexacene," Iscience **19** (2019) 1079.
- <sup>177</sup> E. Busby, T. C. Berkelbach, B. Kumar, A. Chernikov, Y. Zhong, H. Hlaing, X. Y. Zhu, T. F. Heinz, M. S. Hybertsen, M. Y. Sfeir, D. R. Reichman, C. Nuckolls, and O. Yaffe, "Multiphonon Relaxation Slows Singlet Fission in Crystalline Hexacene," Journal of the American Chemical Society **136** (2014) 10654.
- <sup>178</sup> Z. Birech, M. Schwoerer, J. Pflaum, and H. Schwoerer, in *Frontiers in Optics 2014* (Optica Publishing Group, Tucson, Arizona, 2014), p. FTu1G.8.
- <sup>179</sup> F. Weber, and H. Mori, "Machine-learning assisted design principle search for singlet fission: an example study of cibalackrot," npj Computational Materials **8** (2022) 176.